Cell Reports

Article

Snail maintains the stem/progenitor state of skin epithelial cells and carcinomas through the autocrine effect of matricellular protein Mindin

Graphical abstract

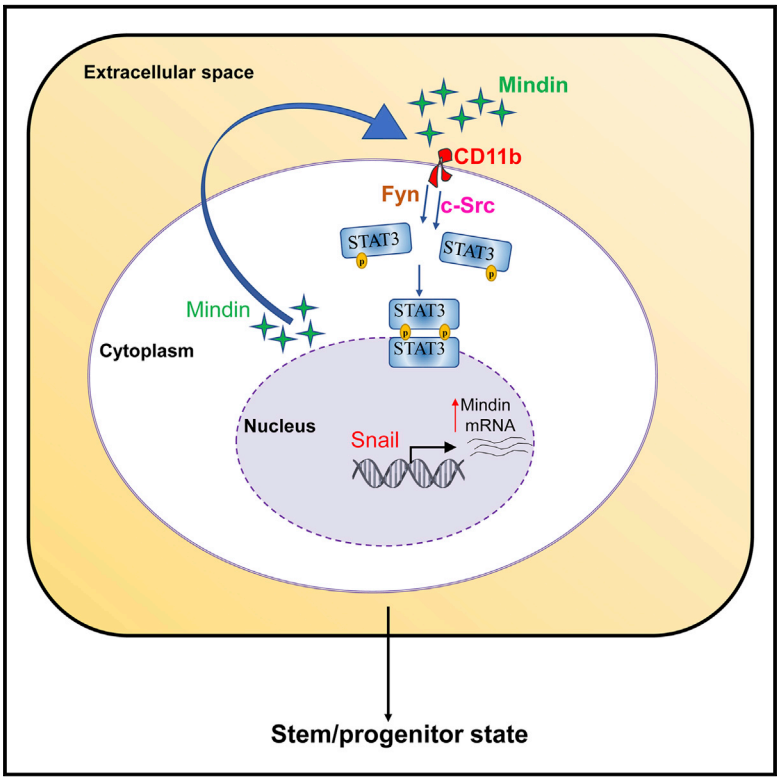

Highlights

- Non-EMT role of Snail in maintaining stemness of epithelial cells
- Snail-expressing keratinocytes secrete Mindin to maintain stem/progenitor state
- $\alpha_M\beta_2$ on epidermal keratinocytes acts as a ligand for Mindin
- The Mindin signaling pathway is crucial for cancer stem cell repopulation of tumors

Authors

Krithika Badarinath, Binita Dam, Sunny Kataria, ..., You-Wen He, Sudhir Krishna, Colin Jamora

Correspondence

colinj@instem.res.in

In brief

Cancer stem cells are important for tumor initiation, growth, metastasis, and relapse after chemotherapy. Badarinath et al. report the discovery of a potential therapeutic target to eliminate cancer stem cells in skin tumors and potentially other tumors in the body.

Badarinath et al., 2022, Cell Reports *40*, 111390
September 20, 2022
https://doi.org/10.1016/j.celrep.2022.111390

CellPress

Cell Reports

CellPress
OPEN ACCESS

Article

Snail maintains the stem/progenitor state of skin epithelial cells and carcinomas through the autocrine effect of matricellular protein Mindin

Krithika Badarinath,[1,2,10,11] Binita Dam,[2,3] Sunny Kataria,[1,2] Ravindra K. Zirmire,[2,4] Rakesh Dey,[2] Gaurav Kansagara,[2,3] Johan Ajnabi,[2] Akshay Hegde,[2,4] Randhir Singh,[5] Tafheem Masudi,[2,12] Janani Sambath,[3,6] Sasikala P. Sachithanandan,[1] Prashant Kumar,[3,6,7] Akash Gulyani,[5,13] You-Wen He,[8] Sudhir Krishna,[1,9] and Colin Jamora[2,14,*]

[1]National Centre for Biological Sciences (TIFR), Bangalore 560065, India
[2]IFOM-inStem Joint Research Laboratory, Centre for Inflammation and Tissue Homeostasis, Institute for Stem Cell Science and Regenerative Medicine (inStem), Bangalore 560065, India
[3]Manipal Academy of Higher Education (MAHE), Manipal 576104, India
[4]School of Chemical and Biotechnology, Shanmugha Arts, Science, Technology and Research Academy (SASTRA) University, Thanjavur, Tamil Nadu 613401, India
[5]Integrative Chemical Biology, Institute for Stem Cell Science and Regenerative Medicine (inStem), Bangalore 560065, India
[6]Institute of Bioinformatics, International Technology Park, Bangalore 560066, India
[7]Karkinos Healthcare Pvt Ltd., Vidyavihar(W), Mumbai 400086, India
[8]Department of Immunology, Duke University Medical Center, Durham, NC, USA
[9]School of Interdisciplinary Life Sciences, Indian Institute of Technology Goa, Ponda 404401, India
[10]Present address: Department of Medical Oncology and Center for Functional Cancer Epigenetics, Dana-Farber Cancer Institute, Boston, MA 02215, USA
[11]Present address: Departments of Medicine, Brigham & Women's Hospital and Harvard Medical School, Boston, MA 02115, USA
[12]Present address: Department of Medical Biochemistry and Cell Biology, Institute of Biomedicine at the Sahlgrenska Academy, University of Gothenburg, 41390 Gothenburg, Sweden
[13]Present address: Department of Biochemistry, School of Life Sciences, University of Hyderabad, Central University Post, Prof. C.R. Rao, Gachibowli, Hyderabad, Telengana 500046, India
[14]Lead contact
*Correspondence: colinj@instem.res.in
https://doi.org/10.1016/j.celrep.2022.111390

SUMMARY

Preservation of a small population of cancer stem cells (CSCs) within a heterogeneous carcinoma serves as a paradigm to understand how select cells in a tissue maintain their undifferentiated status. In both embryogenesis and cancer, Snail has been correlated with stemness, but the molecular underpinning of this phenomenon remains largely ill-defined. In models of cutaneous squamous cell carcinoma (cSCC), we discovered a non-epithelial-mesenchymal transition function for the transcription factor Snail in maintaining the stemness of epidermal keratinocytes. Snail-expressing cells secrete the matricellular protein Mindin, which functions in an autocrine fashion to activate a Src-STAT3 pathway to reinforce their stem/progenitor phenotype. This pathway is activated by the engagement of Mindin with the leukocyte-specific integrin, CD11b (ITGAM), which is also unexpectedly expressed by epidermal keratinocytes. Interestingly, disruption of this signaling module in human cSCC attenuates tumorigenesis, suggesting that targeting Mindin would be a promising therapeutic approach to hinder cancer recurrence.

INTRODUCTION

Tissue morphogenesis, homeostasis, regeneration, repair, and disease are critically dependent on the maintenance of a limited population of resident stem cells (Blanpain and Fuchs, 2006). The ability of these cells to self-renew and differentiate provides a stable pool of progenitor cells to rebuild tissues for regeneration or following wounding (Xia et al., 2018). Deregulation of these stem cells underlies many hyperplastic diseases such as cancer and can be a platform to study the signaling pathways that regulate stem cell behavior within a tissue. Stem cells in a carcinoma, called the cancer stem cells (CSCs), are few in number and play a critical role in cancer initiation, maintenance, drug resistance, and progression. Interestingly, the CSC population is not static but increases in number with tumor grade, thereby increasing tumor heterogeneity (Li et al., 2013; Yu, 2012). Moreover, CSCs are usually quiescent, have increased proficiency in DNA repair, disable their apoptotic pathways, and express increased levels of efflux transporters (Phi et al., 2018). These characteristics render CSCs capable of evading standard

cytotoxic therapies (Li et al., 2021). A similarity between tissue stem cells and CSCs is their residence within a niche, a specialized microenvironment, that regulates stem cell behavior by providing cues in the form of both cellular contacts and soluble factors (Sun et al., 2019). Soluble factors can arise from the tumor cell itself as well as from cells in the tumor stroma (Plaks et al., 2015). Examples of growth factors and cytokines that maintain the undifferentiated state of cells are Hedgehog, Wnt, and Notch, while stemness-promoting intracellular signaling pathways utilize JAK/STAT, PI3K/phosphatase, Hippo, and NF-κB (Matsui, 2016; Plaks et al., 2015). Identification of cancer-specific components in these common signaling pathways that can be targeted to inhibit tumorigenesis while sparing physiological processes would thus be an ideal therapy.

Given the importance of CSCs, many studies have focused on understanding their role and regulation in tumorigenesis. One open question is how the few CSCs are maintained in a tumor mass among a sea of differentiating cells. To answer this question, we utilized a transgenic mouse model based on the overexpression of Snail in epidermal keratinocytes (*K14-Snail Tg*), which reproduces many of the cardinal features of squamous cell carcinoma (Du et al., 2010). Snail is a transcription factor that is well known for its function in inducing an epithelial-mesenchymal transition (EMT) during embryogenesis (Murray and Gridley, 2006) and hair morphogenesis (Jamora et al., 2005), and it is overexpressed in many carcinomas (Fan et al., 2012; Goossens et al., 2017; Mani et al., 2009). Interestingly, there is a strong correlation between Snail expression with the number of CSCs (Hojo et al., 2018; Ma et al., 2017; Zhou et al., 2014) as well as tumor aggressiveness (Smith et al., 2014; Zheng et al., 2015). Several proposals have been formulated to explain the connection between Snail and CSCs including the ability of EMTs to promote de-differentiation of cells to acquire stem cell properties (Wang and Unternaehrer, 2019). Moreover, extracellular signals such as TGFβ and Wnt, which are known to promote CSC production, are dependent on EMT drivers such as Snail and Twist (Scheel et al., 2011). Despite these correlations, the molecular mechanism by which Snail specifically regulates the stemness and number of CSCs remains largely unknown.

In the Snail Tg mouse and cutaneous squamous cell carcinoma (cSCC) cells, we unexpectedly find that the transcription factor Snail maintains stemness of keratinocytes by creating a niche via the secretion of the matricellular protein Mindin. In an autocrine fashion, extracellular Mindin utilizes the Src family of kinases (SFKs) to activate STAT3 to reinforce the stem/progenitor phenotype. Disruption of this signaling module in human cSCC impedes tumor formation in xenograft assays. Our findings reveal a novel non-EMT role for Snail that is mediated by Mindin released into the extracellular milieu. The broad expression of these signaling components in various carcinomas suggest that they would be an effective target for therapeutic intervention.

RESULTS

Overexpression of *Snail* reinforces the stem/progenitor characteristics in epidermal keratinocytes *in vitro*

Given Snail's canonical function in inducing an EMT, we tested if this process was activated in the *K14-Snail* transgenic (Snail Tg) skin by three different criteria: (1) lineage tracing assay (Rana et al., 2022), (2) immunofluorescence at postnatal day 9 (P9) to examine cells co-expressing epithelial (keratin 5) and mesenchymal (vimentin [Figure 1A] and collagen [Figure S1A]) markers, and (3) maintenance of distinct epithelial and mesenchymal compartments delineated by the basement membrane marked by laminin 5 (Figure 1A). Altogether, this analysis unexpectedly revealed that transgenic expression of *Snail* in epidermal keratinocytes *in vivo* is insufficient to induce an EMT. To validate these surprising observations, we examined whether primary keratinocytes isolated from the Snail Tg skin exhibited features of EMT *in vitro*. We computed the EMT score for each sample using transcriptome data to estimate the EMT phenotype (Tan et al., 2014) (Figure 1B). The EMT scores of both wild-type (WT) and Snail Tg cells were distributed between −0.18 and −0.20, indicating no difference between the two sample sets (Figure S1B). Consistent with the *in vivo* data, we found that primary keratinocytes isolated from the Snail Tg skin retain their epithelial characteristics *in vitro*.

We previously observed that the Snail Tg skin recapitulated many hallmarks of cSCC (Du et al., 2010). In particular, there was robust epidermal hyperplasia with an expansion of the basal layer (Du et al., 2010), which harbors the stem/progenitor cells of the epidermis. To determine how Snail is stimulating the expansion of the basal layer of keratinocytes (Du et al., 2010) in a non-EMT fashion, we analyzed the transcriptome profile of the transgenic keratinocytes for potential clues. Gene ontology of differentially expressed genes (Figure S1C) revealed that the regulation of cell proliferation and cell differentiation are the top two biological processes that are affected in the Snail Tg keratinocytes (Figure 1C). qPCR analysis confirmed that there were elevated levels of proliferation-associated genes and decreased expression of differentiation genes in Snail Tg keratinocytes (Figure 1D). Thus, the underlying expansion of the basal layer of the Snail Tg skin may be accomplished by the hyperproliferation of keratinocytes and/or the inhibition of differentiation. Interestingly, we found that primary Snail Tg keratinocytes do not display a higher proliferation rate *in vitro* compared with WT cells (Figure S1D). In addition, we assessed the proliferative status of epidermal keratinocytes in the skin *in vivo* and in cultured primary keratinocytes by tracking the proliferation antigen Ki67. An increase in the number of Ki67+ cells was observed in the Snail Tg skin at both P9 and P60 compared with their WT counterpart (FigureS1E). However, there was no difference observed between the primary WT and Snail Tg keratinocytes (Figure S1F). This is consistent with our previous report that implicated proliferation in the Snail Tg skin as secondary to inflammation (Du et al., 2010). These observations suggest that increased expression of proliferative genes in primary Snail Tg keratinocytes prime the cells to proliferate, while they need an inflammatory component to actively enter the cell cycle. Interestingly, the transcriptome of the transgenic cells indicates that genes involved in stem cell population maintenance are upregulated (Figures 1E and S1G). Consistent with the *in vitro* results, freshly isolated integrin $\alpha6^+$ epidermal keratinocytes from the skin also exhibited a similar expression pattern of the genes involved in proliferation, differentiation, and stem cell maintenance (Figure S1H). Furthermore, we analyzed the expression profile of other EMT transcription factors such as Twist and Slug, involved in maintenance of

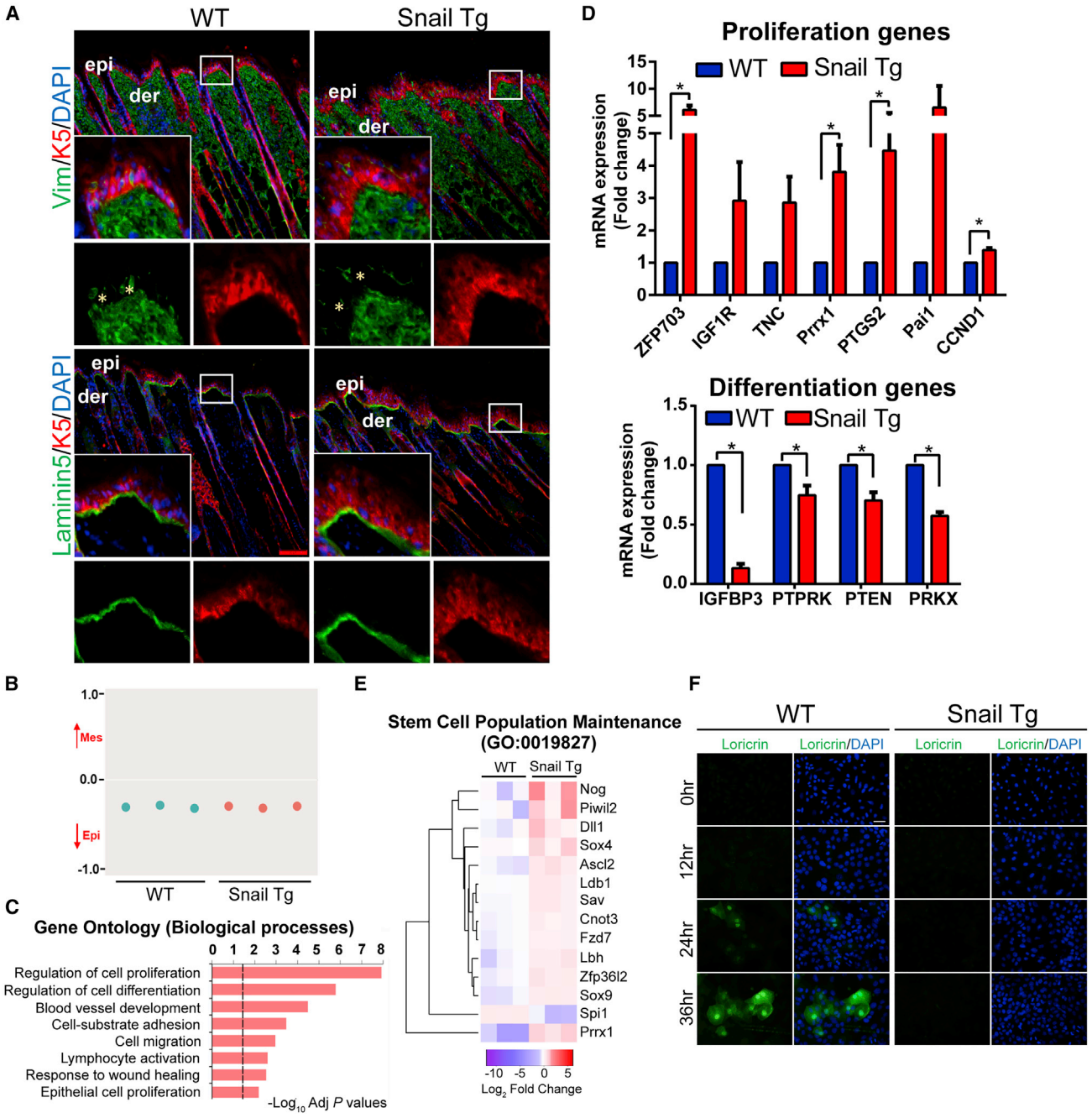

Figure 1. Overexpression of Snail reinforces the stem/progenitor characteristics *in vitro*

(A) Immunofluorescence of cells in the skin. Top row: Vimentin (green) to mark the mesenchymal cells and keratin 5 (red) to mark the basal epidermal keratinocytes and outer root sheath of hair follicles in wild-type (WT) and Snail transgenic (Tg) skin. Bottom row: Laminin 5 (green) marks the basal lamina and keratin 5 is in red. Insets are magnified views of the boxed areas of the epidermis. Scale bar, 50 μm.

(B) EMT score calculated using the transcriptome data of WT and Snail Tg keratinocytes.

(C) Gene ontology of the differentially expressed genes in Snail Tg keratinocytes.

(D) qPCR of proliferation and differentiation associated genes (n = 3).

(E) Heatmap of genes corresponding to the Gene Ontology term "stem cell population maintenance."

(F) Differentiation potential of WT and Snail transgenic keratinocytes in the calcium switch assay using loricrin (green) as a marker of differentiation. Scale bar, 20 μm (n = 3). Data represent the mean ± SEM. p values were calculated using paired Student's t test (D). *$p < 0.05$, ***$p < 0.001$. See also Figure S1.

stemness (Jung and Yang, 2015; Mistry et al., 2014). An increase in the levels of Twist was observed in the Snail Tg keratinocytes; however, Slug was significantly decreased compared with its WT counterpart (Figure S1I). These results are consistent with previous observations that upregulation of Twist promotes stemness (Beck et al., 2015) and the overexpression of Snail leads to the downregulation of Slug (Gingold et al., 2014) (Figure S1I). One prediction that can be made if Snail maintains the stem/progenitor characteristic of basal epidermal keratinocytes, the transgenic cells should be resistant to the differentiation. To test this, we assessed the differentiation potential of Snail Tg keratinocytes *in vitro* by the classical calcium switch assay (Bikle et al., 2012). Unlike WT cells, we observed that the Snail Tg keratinocytes fail to express the differentiation marker loricrin even after 36 h of differentiation (Figure 1F). Moreover, the nuclear to cytoplasmic ratio (NCR) of WT and Snail Tg cells at different time points along the differentiation process was analyzed. Interestingly, the Snail Tg keratinocytes displayed a higher NCR even after 36 h of differentiation, consistent with a stem cell phenotype, while the WT cells showed a decrease (Figure S1J). This is consistent with our previous study that reported that the Snail Tg epidermis exhibits a spatial delay in the differentiation process (Jamora et al., 2005). In total, these results reveal a novel non-EMT function of Snail in maintaining stem/progenitor characteristics in epidermal keratinocytes of the basal layer.

Epidermal Snail expression expands the epidermal stem/progenitor cell population *in vivo*

We previously reported an expansion of the basal layer of the Snail transgenic epidermis that contributes to the thickening of the tissue (Du et al., 2010). The basal layer is the home of epidermal stem/progenitor cells that normally fuel the regeneration of the epidermis. To determine if an expansion in the number of these cells contributes to epidermal hyperplasia, we analyzed two widely utilized markers of these epidermal stem/progenitors cells: CD49f (Krebsbach and Villa-Diaz, 2017; Schober and Fuchs, 2011; Ye et al., 2017) and p63 (Blanpain and Fuchs, 2007; Koster et al., 2005). Immunohistochemical analysis of these markers showed an increased number of epidermal stem/progenitor cells in the P9 Snail Tg epidermis compared with its WT counterpart (Figure 2A). These results were intriguing since the basal layer (marked by keratin 5) is the exclusive home of the epidermal stem/progenitor cells, and their delamination from this layer into the suprabasal layers is generally considered a signal to lose their stemness and enter the terminal differentiation program (Fuchs, 2008). Nevertheless, we found that there is a substantial increase in the number of p63-positive cells in the suprabasal layers of the Snail Tg epidermis (Figure S2A). Together with previous findings of an expansion of keratin 5 staining in the transgenic skin (Du et al., 2010; Jamora et al., 2005), this suggests that there is an expansion of the basal layer into the suprabasal domain. In addition, generic markers of stem cells such as *Oct4, Sox2*, and *Nanog* were likewise upregulated in the Snail Tg skin (Figures S2B and S2C). Furthermore, ultrastructural analysis of the suprabasal keratinocytes of the epidermis in the Snail Tg skin revealed pleomorphic nuclei with diffused heterochromatin and multiple nucleoli, which are morphological features of stem cells (Figure 2B).

Given the expansion of the epidermal stem/progenitor cells found *in vivo*, we investigated whether this phenotype is a cell autonomous effect of *Snail* overexpression or secondary to inflammation. As we have previously shown, inflammation is responsible for epidermal keratinocyte proliferation in the Snail transgenic skin, but it was not involved in the maintenance of the stem cell characteristics of basal epidermal keratinocytes (Du et al., 2010). To probe whether stemness is a cell autonomous function of *Snail*, we cultured primary keratinocytes from WT and Snail Tg skin and analyzed various characteristics of stemness. In colony forming assays, which score for the self-renewal capacity of stem cells, Snail Tg keratinocytes exhibited a higher number of colonies over several seedings compared with WT cells (Figure 2C). Other features of CSCs such as increased NCR (Yang et al., 2020) (Figure 2D) and expression of stem cell genes (Figure 2E) are higher in Snail Tg keratinocyte relative to its WT counterpart. These observations are consistent with reports of a strong positive correlation between Snail expression and the undifferentiated state of cancer cells (Fan et al., 2012; Ma et al., 2017). Our *in vitro* findings were further validated using a xenograft assay, which is the gold standard in defining a cell as a stem cell. We grafted 0.25×10^6 Snail Tg keratinocytes in immunocompromised (NSG) mice with WT cells as control. Two months after grafting, ~90% of mice formed tumors with Snail Tg keratinocytes compared with 0% with control cells (Figure 2F). Interestingly, when we serially grafted the cells isolated from the first graft (first generation) of Snail Tg tumors, we observed that ~75% of the grafts formed second-generation tumors. Moreover, the tumors formed by the Snail Tg cells displayed elevated levels of pro-tumor genes compared with primary WT and Snail Tg keratinocytes (Figure S1D). These results suggest that *Snail* overexpression not only upregulates markers associated with stem/progenitor cells, but it also endows them stem cell capabilities.

Snail-mediated stem/progenitor cell maintenance is dependent upon STAT3 activation

While many studies have firmly established an association of Snail expression with heightened cancer stem-like properties (De Craene et al., 2014; Hojo et al., 2018), the mechanism underlying this correlation nevertheless remains elusive. An essential component that maintains the stemness of a variety of cells is the active form of STAT3 (phosphorylated STAT3, pSTAT3) (Galoczova et al., 2018; Raz et al., 1999). Previously, we reported an increased activation (phosphorylation) of STAT3 in the Snail Tg epidermis compared with its WT counterpart (Du et al., 2010). To determine if STAT3 activation is a cell autonomous effect, we measured both total and activated STAT3 levels in primary WT and Snail transgenic keratinocytes. Interestingly, we observed that Snail expression is sufficient to increase the levels of both total STAT3 protein as well as pSTAT3 (Figures 3A and 3B and S3A–S3C). To assess the functional relevance of this active pSTAT3, we treated WT and Snail Tg keratinocytes with BP-1-102, a small molecule inhibitor, which inhibits the phosphorylation, dimerization, and subsequent nuclear translocation of STAT3 (Zhang et al., 2012). We found that inhibition of STAT3 phosphorylation by ~50% in Snail transgenic keratinocytes (Figures S3D–S3F) substantially suppressed their self-renewal

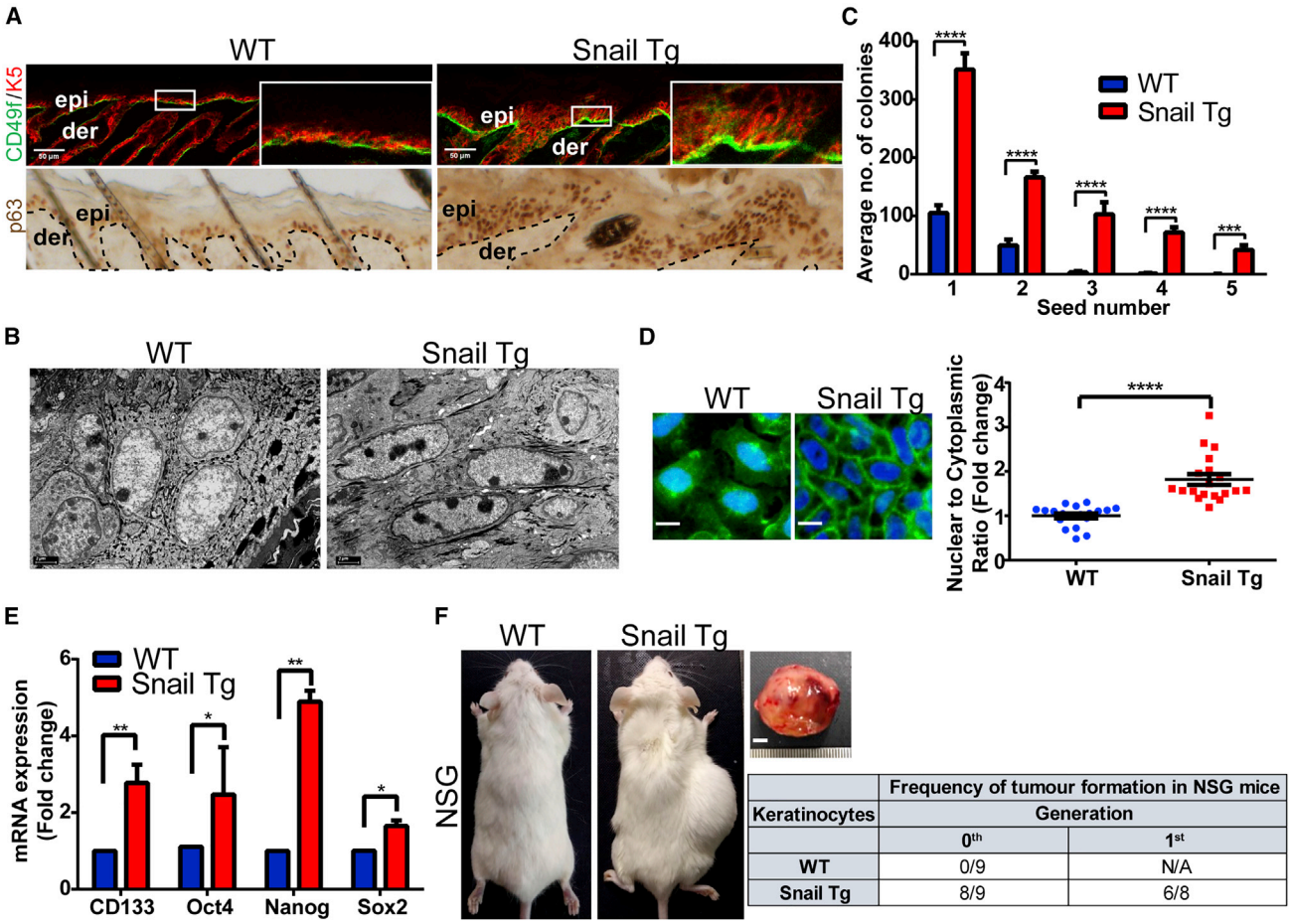

	Frequency of tumour formation in NSG mice	
Keratinocytes	Generation	
	0th	1st
WT	0/9	N/A
Snail Tg	8/9	6/8

Figure 2. Epidermal Snail expression expands the epidermal stem/progenitor cell population in vivo

(A) Immunohistochemistry of CD49f and p63 marking the stem/progenitor cells in WT and Snail Tg skin. Dotted line represents the basement membrane, which separates the epidermis (epi) from the underlying dermis (der). Scale bar, 50 μm.

(B) Ultrastructural analysis demonstrating increased number of nucleoli and dispersed chromatin in the Snail Tg suprabasal keratinocytes compared WT (n = 2). Scale bar, 2 μm.

(C) Colony formation assay on WT and Snail Tg keratinocytes. 1,000 cells were plated per well for each seeding, and colonies numbers were quantified after 7 days (n = 3/seeding).

(D) Analysis of nuclear to cytoplasmic ratio (NCR) in WT and Snail Tg epidermal keratinocytes. Left panel: Immunofluorescence of WGA (cell membrane) and DAPI (nucleus). Scale bar, 5 μm Right panel: Quantification showing higher NCR in Snail Tg compared with WT keratinocytes.

(E) WT (blue) and Snail Tg (red) keratinocytes analyzed for the stem cell genes CD133, Oct4, Sox2, and Nanog by qPCR (n = 3).

(F) Tumor-forming capacity of WT and Snail Tg keratinocytes injected in NSG animals. Image shows tumor formed by the Snail Tg keratinocytes 2 months after injection. Scale bar, 5 mm. The table summarizes the number of tumors formed by WT and Snail Tg cells in the initial injection and the first generation derived from cells from the tumor developed in the initial injection. Data represent the mean ± SEM. p values were calculated using two-tailed t test (C and E) and Student's t test (D). *p < 0.05, **p < 0.01, ***p < 0.001, and ****p < 0.0001. See also Figure S2.

capacity (Figure 3C) and stem cell-associated genes (Figure 3D). In addition, the increased NCR and the expression of the cancer stem cell marker CD44 (Figures 3E, 3F and S3G) were significantly reduced to near WT levels upon STAT3 inhibition.

We extended this study to understand if active pSTAT3 was essential for Snail's impact on keratinocyte stemness *in vivo*. The STAT3 inhibitor was applied topically on the back skin of newborn WT and Tg animals every 2 days up to day 7. Analysis of the skin revealed that the increase in the number of layers positive for keratin 5 in the Snail Tg epidermis was significantly reduced upon STAT3 inhibition (Figures 3G and 3H). Further, we found that the reduction of the thickened basal layer correlated with a decrease in the number of p63-positive stem/progenitor cells (Figures 3I and S3H). Collectively, both *in vitro* and *in vivo* studies indicate that the activation of STAT3 is crucial for Snail-mediated stem/progenitor characteristics of epidermal keratinocytes.

Mindin secreted by Snail Tg keratinocytes activates STAT3 in an autocrine fashion

We further sought to elucidate the molecular pathway linking Snail with STAT3 activation. STAT3 activation is regulated via

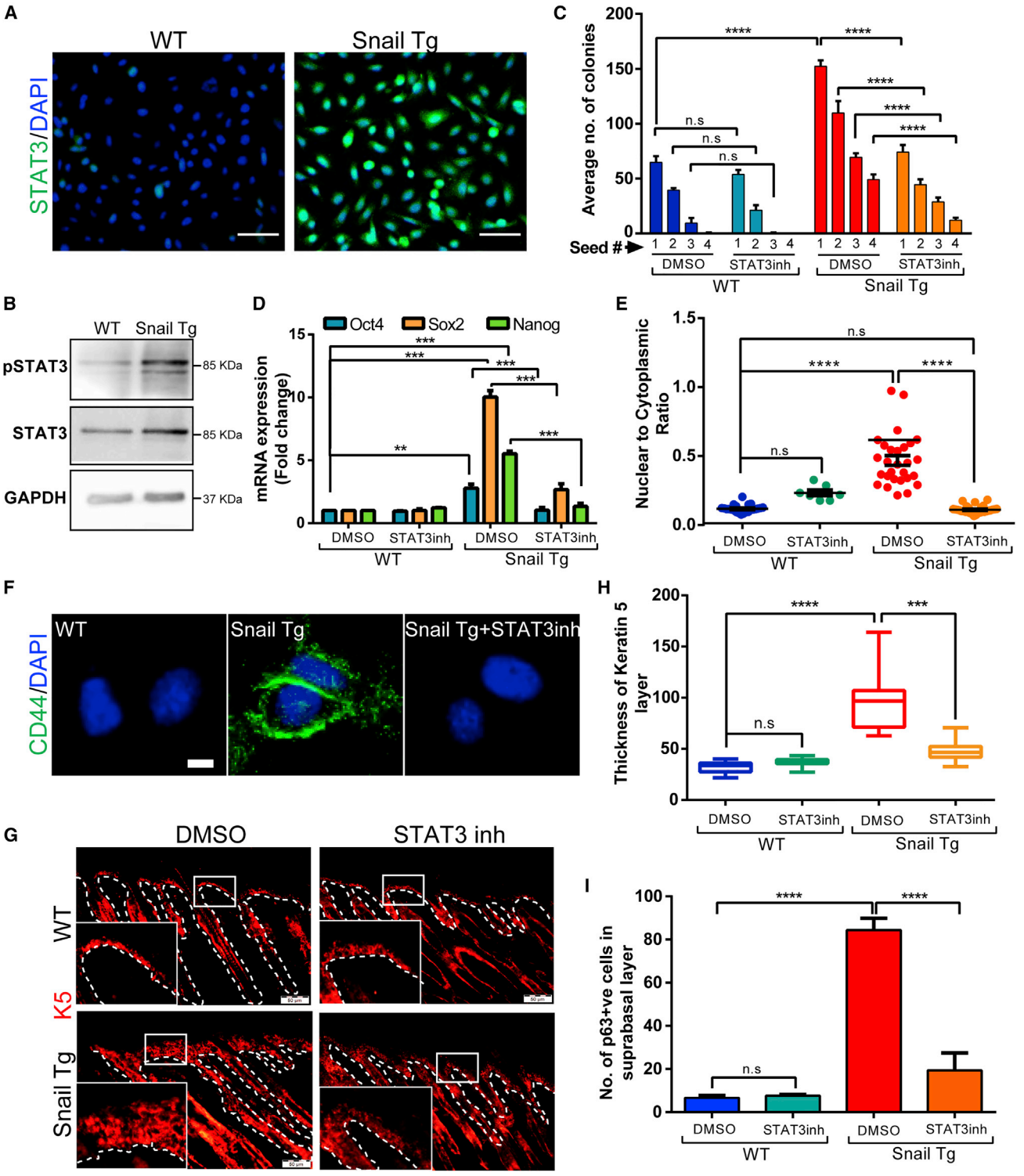

Figure 3. Snail-mediated stem/progenitor cell maintenance is dependent upon STAT3 activation

(A) Immunofluorescence of total STAT3 (green) and DAPI (blue) on WT and Snail Tg keratinocytes. Scale bar, 10 μm.

(B) Western blot for phosphorylated STAT3 (pSTAT3) and total STAT3 in WT and Snail Tg keratinocytes. GAPDH is the loading control.

(C) Number of colonies formed by WT and Snail Tg keratinocytes in the presence or absence of STAT3 inhibitor or vehicle control, DMSO. n = 3 for each seeding.

(D) qPCR analysis of stem cell gene expression in WT and Snail Tg keratinocytes upon STAT3 inhibition (n = 3).

(E) Nuclear to cytoplasmic ratio of WT and Snail Tg keratinocytes upon STAT3 inhibition (n = 3).

(legend continued on next page)

receptor tyrosine kinases (Grandis et al., 1998) or by non-receptor tyrosine kinases (Bowman et al., 2000), which are stimulated by multiple extracellular ligands (Rébé et al., 2013). We therefore postulated that keratinocytes expressing Snail secrete proteins to the extracellular milieu capable of activating STAT3 in an autocrine fashion. To test this hypothesis, we treated primary keratinocytes with conditioned media obtained from cultured WT or Snail Tg keratinocytes and assessed the levels of pSTAT3. Snail Tg conditioned media increased the levels of activated STAT3 compared with WT conditioned media (Figures 4A and S4A). We next embarked upon identifying the specific component(s) in the Snail Tg conditioned media that is responsible for this effect. We have profiled the secretome of the Snail transgenic keratinocytes and have identified several unique proteins that were not present in conditioned media prepared from WT keratinocytes. Previous work from our lab has shown that these secreted proteins such as fibulin-5 (Nakasaki et al., 2015), PAI-1 (Pincha et al., 2018), and Mindin (Rana et al., 2022) have important roles in promoting dermal fibrosis in the transgenic skin. Interestingly, among these secreted proteins, Mindin has attracted recent attention due to its upregulation in numerous carcinomas (Jin et al., 2017; Lucarelli et al., 2013; Ni et al., 2019; Simon et al., 2007; Zhang et al., 2015), which underlies its use as a potential diagnostic biomarker. Therefore, we inspected the levels of Mindin in the Snail Tg skin, and we observed increased levels of secreted Mindin in non-permeabilized Snail Tg skin compared with WT tissue (Figure S4B). Likewise, Mindin RNA is upregulated in the Snail Tg keratinocytes compared with the WT cells (Figure 4B). To identify if Snail could directly activate Mindin, we analyzed the Mindin promoter and identified the presence of the canonical E-box sequences that are binding domains for Snail (Figure S4C). Interestingly, upon analyzing the ChIP-seq dataset performed on epithelial cells from Schmitges et al. (2016), we observed an enrichment for Snail binding on the Mindin promoter region (Figure S4D). Likewise, analysis of the ChIP-seq dataset from Mistry et al. (2014) performed on keratinocytes revealed the robust binding of another Snail family member (Snail 2) on Mindin promoter region (Figure S4E). Consistent with a role in mediating keratinocyte stemness, the epidermal hyperplasia found in the Snail Tg skin is reduced to almost WT levels when Mindin was genetically ablated (Figures 4C and S4E). However, deletion of Mindin in the WT background did not show any epidermal phenotype and was comparable to the WT skin (Figure S4F). Interestingly, other components in the Snail conditioned media, namely PAI-1 (Pincha et al., 2018) and fibulin-5 (Nakasaki et al., 2015), have no effect on the epidermal hyperplasia in the Snail transgenic mouse. Moreover, we observed that the expansion of the stem/progenitor population in the epidermis of Snail Tg skin is reduced in the absence of Mindin (Figure 4C). Further, we examined if Mindin is the link between Snail and STAT3 activation. In Snail Tg/Mindin knockout (KO) skin, there was a significant reduction in the levels of activated STAT3 compared with the Snail Tg skin (Figure 4C). Concomitant with the *in vivo* observations, Snail Tg keratinocytes lacking Mindin showed reduced self-renewal capacity (Figure 4D), decreased expression of stem cell genes (Figure 4E), and a lower NCR (Figure 4F). Moreover, the level of activated STAT3 in the Snail Tg/Mindin KO keratinocytes was lower compared with Snail Tg cells (Figure S4G).

To test the sufficiency of Mindin to activate STAT3, we treated WT keratinocytes with recombinant Mindin (rMindin) and analyzed the levels of phosphorylated protein. We observed that rMindin treatment resulted in elevated levels of pSTAT3 compared with buffer control treatment (Figures 4G, S4H, and S4I)). We further investigated if Mindin is also sufficient to enhance the stem/progenitor characteristics in WT cells. We observed that Mindin-treated keratinocytes exhibited an increased colony-forming capacity (Figure S4J), a higher NCR (Figure S3K), and elevated expression of stem cell markers (Figures S4L and S4M) in a STAT3-dependent manner. In summary, Mindin is sufficient to endow epidermal keratinocytes with stem/progenitor characteristics through the activation of STAT3 (Figure 4H).

Src family of kinases mediates Mindin-dependent activation of STAT3

We then investigated the kinase responsible for phosphorylating STAT3 downstream of Mindin signaling. Mindin is reported to be a ligand for integrins on immune cells, which in turn activates STAT3 via SFKs (Jia et al., 2005; Xue et al., 2010). To test whether this same pathway is active in epidermal keratinocytes, we assessed the levels of activated (phosphorylated) Src (pSrc) in Snail Tg versus WT keratinocytes with a phospho-pan-Src antibody (Figures 5A and S5A). Snail Tg keratinocytes exhibited a 2-fold increase in activated Src compared with its WT counterpart. To examine whether Mindin was sufficient to activate Src, we treated WT keratinocytes with rMindin and observed a 3-fold increase in Src activation (Figures 5B and S5B).

A broad-spectrum pharmacological inhibitor of SFKs led to a reduction in phosphorylated STAT3 levels in Snail Tg keratinocytes (Figures S5C and S5D). We then explored which specific SFK member(s) is responsible for Mindin-mediated STAT3 activation using a knockdown approach. shRNA-mediated knockdown was performed for each of the three ubiquitously expressed SFK members (*c-Src, Fyn*, and *Yes*) in Snail Tg keratinocytes (Figure S5E). Knocking down either *Fyn* or *c-Src* resulted in a significant reduction in the levels of pSTAT3 (Figures 5C and 5D). Furthermore, to functionally examine the effect of these

(F) Immunofluorescence of CD44 (green) in WT, Snail Tg, and Snail Tg + STAT3inh cells. Scale bar, 2 μm.

(G) Immunofluorescence panels showing stem/progenitor layer of the epidermis marked by keratin 5 in red on WT and Snail Tg skin upon STAT3 inhibition. Dotted line represents the basement membrane, which separates the epidermis (epi) from the underlying dermis (der). Insets in each panel are magnified views of the boxed areas of the epidermis. Scale bar, 50 μm.

(H) Thickness of the stem/progenitor layer in the WT and Snail Tg skin after STAT3 inhibition, n = 2 animals each.

(I) Number of p63-positive cells in the suprabasal layer of the WT and Snail Tg epidermis after STAT3 inhibition (n = 3). Data represent the mean ± SEM. p values were calculated using either the two-way ANOVA followed by Tukey's post hoc analysis (C and D) or one-way ANOVA followed by Tukey's post hoc analysis (E, H, and I). **p < 0.01, ***p < 0.001, ****p < 0.0001, and n.s = not significant. See also Figure S3.

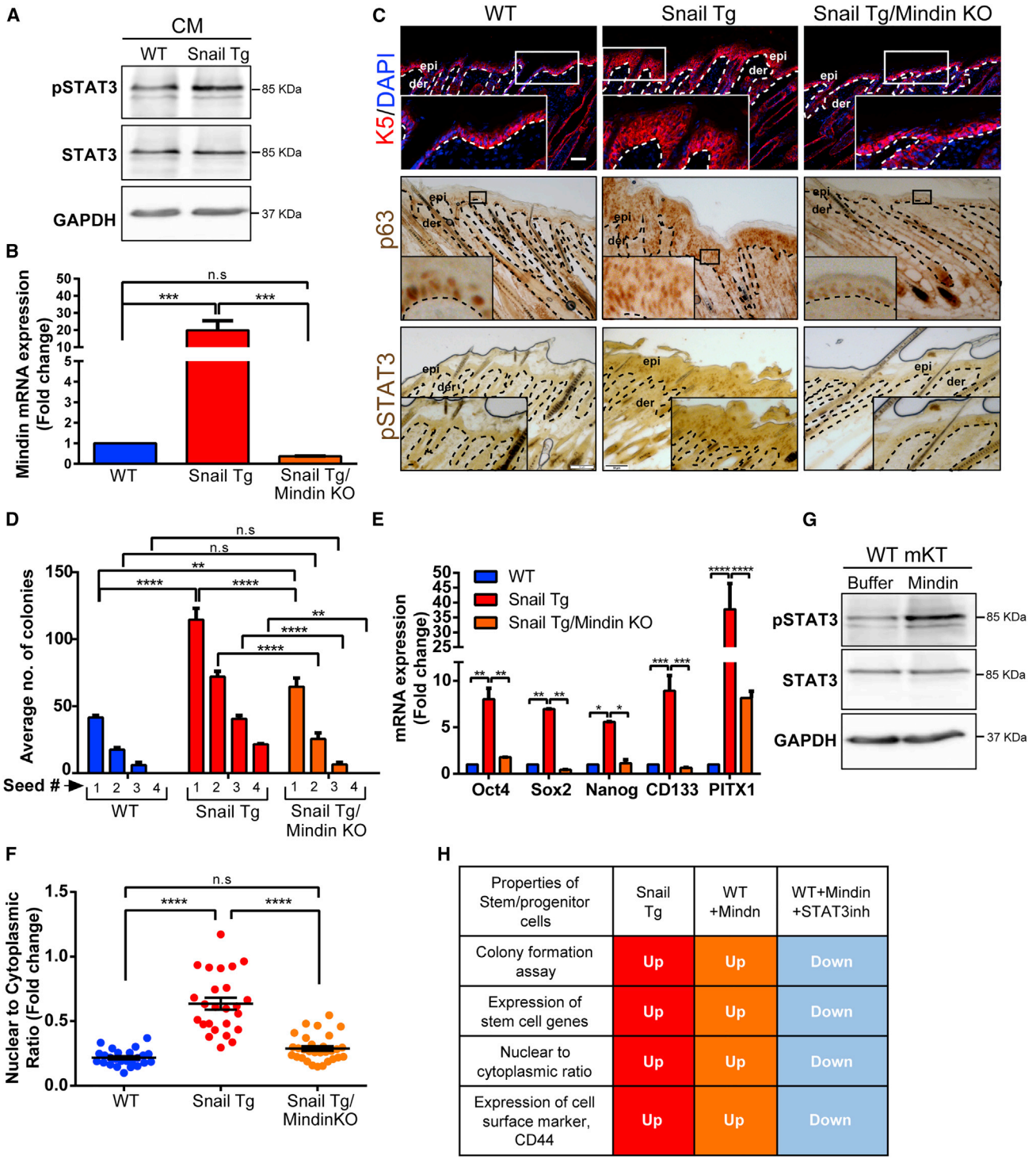

Properties of Stem/progenitor cells	Snail Tg	WT +Mindn	WT+Mindin +STAT3inh
Colony formation assay	Up	Up	Down
Expression of stem cell genes	Up	Up	Down
Nuclear to cytoplasmic ratio	Up	Up	Down
Expression of cell surface marker, CD44	Up	Up	Down

Figure 4. Secreted Mindin by Snail Tg keratinocytes activates STAT3 in an autocrine fashion

(A) Western blot for pSTAT3 and total STAT3 in WT cells treated with conditioned media (CM) from WT or Snail Tg keratinocytes. GAPDH = loading control (n = 3).

(B) qPCR of Mindin mRNA levels in WT, Snail Tg, and Snail Tg/Mindin KO keratinocytes (n = 3).

(C) Top row: Immunofluorescence of keratin 5 (K5) in red in WT, Snail Tg, and Snail Tg/Mindin KO skin. Scale bar, 30 μm. Middle row: Immunohistochemistry of p63 on WT, Snail Tg, and Snail Tg/Mindin KO skin. Bottom row: Immunohistochemistry of pSTAT3 in WT, Snail Tg, and Snail Tg/Mindin KO skin. Dotted line represents the basement membrane, which separates the epidermis (epi) from the underlying dermis (der). Scale bar, 50 μm.

(D) Average number of colonies formed by WT, Snail Tg, and Snail Tg/Mindin KO keratinocytes (n = 3).

(legend continued on next page)

knockdowns, we assessed their impact on the colony-forming capacity of Snail Tg cells. Reduced levels of either *Fyn* or *c-Src* resulted in fewer colonies, while the *Yes* knockdown showed a mild effect (Figure 5E). Interestingly, cells with lower levels of *Fyn* or *Yes* exhibited a reduced expression of stem cell genes (Figure 5F). Finally, we characterized SFK on the morphological parameters of keratinocyte stemness and found that *Fyn* and *c-Src* knockdown caused a decrease in the NCR, while the *Yes* knockdown had no effect (Figures 5G and S5F). Overall, these results suggest that Mindin-STAT3-mediated stem/progenitor properties are via activation of Src kinases. Notably, *Fyn* appears to have the broadest effect on the stem cell characteristics we analyzed (Figure S5G).

Mindin is required for the maintenance of stem/progenitor characteristics in human cutaneous squamous cell carcinoma

Although Mindin has been proposed to be a biomarker for certain cancers such as ovarian (Simon et al., 2007), prostate (Lucarelli et al., 2013), and lung adenocarcinoma (Yuan et al., 2017), the precise role of Mindin in skin cancers is yet to be elucidated. Therefore, we sought to determine if Mindin-mediated stemness observed in Snail Tg mouse keratinocytes is operational in human skin cancers. We first inspected the expression pattern of Mindin in various cancers and found it to be upregulated in 12 out of the 18 different cancers that were analyzed (Figure S6A). In addition, a cell line (A388) derived from a patient with cSCC (Conway et al., 1992) expresses higher levels of Snail (Figure S6B), and it also exhibited higher levels of Mindin mRNA (Figure 6A). We proceeded to investigate whether the increase in Mindin levels observed in the cSCC cell has a functional role in maintaining stem/progenitor characteristics. We utilized the CRISPR-Cas9 system to knock down Mindin in cSCC cells (cSCC-KD). cSCC cells that were selected for Mindin KD with puromycin contained a 50% reduction in the mRNA levels of Mindin compared with control cells (Figure S6C). cSCC-KD cells displayed a reduction in the expression levels of stem cell genes (Figure 6B), self-renewal capacity (Figure 6C), and NCR (Figure 6D). Moreover, the trend observed in all these properties could be rescued upon treatment of cSCC-KD cells with rMindin, suggesting that the phenomenon is not an off-target effect of gene editing. Furthermore, we investigated whether the Mindin-mediated Src-STAT3 signaling module is active in human cSCC cells. cSCC-KD cells exhibited reduced pSTAT3 (Figure 6E) and pSrc (Figure 6F) levels compared with the control (Figure 6E). Moreover, the reduction in SFK and STAT3 activation in cSCC-KD cells was reversed upon the treatment with rMindin. In line with these results, stem cell markers associated with the cSCC cells also decreased in the cSCC-KD cells (Figures 6G and 6H).

In xenograft assays, cSCCs formed tumors in 5/5 mice, while the cSCC-KD cells formed tumors in 7/10 mice. However, the size of the tumors that formed with the cSCC-KD cells were substantially smaller compared with their parental cSCC cells (Figure 6I). In addition to their size difference, the tumors formed by the cSCC-KD cells unexpectedly appeared to have less vascularization compared with that of the tumors from cSCC cells (Figure 6I). Overall, these results signify that Mindin is a critical player required for the maintenance of stem/progenitor characteristics in human squamous cell carcinoma of skin. In addition, the signaling pathway that Mindin mediates to maintain stem/progenitor characteristics in mouse is conserved in human skin cancer cells.

CD11b mediates Mindin signaling in Snail Tg keratinocytes and cSCC cells

Given that extracellular Mindin can maintain the stem/progenitor phenotype of epidermal keratinocytes, we proceeded to identify its cognate receptor on mouse and human keratinocytes. Though the receptor for Mindin on epithelial cells is unknown, it has been reported that Mindin is a ligand for integrin $\alpha M\beta 2$ (CD11b) and $\alpha 4\beta 1$ on macrophages and neutrophils, respectively (Jia et al., 2005; Xue et al., 2010). It is noteworthy that, similar to Mindin, activation of these integrins also stimulate SFK- and STAT3-containing signaling pathways (Meng and Lowell, 1998). Moreover, CD11b is reported to be upregulated in cancers and positively correlates with tumor progression and metastasis (Alday-Parejo et al., 2019) (Ganguly et al., 2013) (Wu et al., 2021). Surprisingly we observed the expression of integrin CD11b RNA in epidermal keratinocytes even though this integrin is considered to be leukocyte specific (Figures S7A and S7B). The level of CD11b RNA in Snail transgenic keratinocytes was statistically equivalent to that of WT cells (Figure S7A), although the expression of this integrin was ~15-fold higher in SCC cells compared with normal human keratinocytes (Figure S7B). Moreover, analysis of various skin cancer cell lines likewise exhibited higher mRNA expression of CD11b relative to normal epithelial cell lines (Figure S7C). These findings are consistent with recent reports documenting the expression of CD11b on non-leukocytic cells such as in epithelia in ovarian cancer (Saed et al., 2018) and in renal cell carcinoma cells (Boguslawska et al., 2016). Using flow cytometry to examine the surface expression of CD11b on epidermal keratinocytes (marked by integrin $\alpha 6$) in the skin of P9 animals, we found that the percentage of $\alpha 6^+$ cells co-expressing membrane CD11b was reduced in Snail Tg keratinocytes (10.3%) compared with its WT counterpart (19.9%) (Figure 7A). Consistent with this *in vivo* observation, the percentage of cultured primary Snail Tg keratinocytes and cSCC cells expressing surface CD11b was ~50% lower compared with WT mouse keratinocytes and human

(E) mRNA expression of Oct4, Sox2, Nanog, CD133, and PITX1 in wild-type Snail Tg and Snail Tg/Mindin KO keratinocytes (n = 3).
(F) Nuclear to cytoplasmic ratio of WT, Snail Tg, and Snail Tg/Mindin KO keratinocytes (n = 3).
(G) Western blot for pSTAT3 and total STAT3 in WT keratinocytes treated with recombinant Mindin or buffer control. GAPDH is the loading control (n = 3).
(H) Table summarizing the stem/progenitor properties displayed by WT, Snail Tg, WT + Mindin, and WT + Mindin + STAT3inh keratinocytes. "Up" denotes an increase compared with WT, and "Down" denotes a decrease compared with Snail Tg keratinocytes. Data represent the mean ± SEM. p values were calculated using one-way ANOVA followed by Tukey's post hoc analysis (B and F) and two-way ANOVA followed by Tukey's post hoc analysis (D and E). *$p < 0.05$, **$p < 0.01$, ***$p < 0.001$, ****$p < 0.0001$, and n.s represents not significant. See also Figure S4.

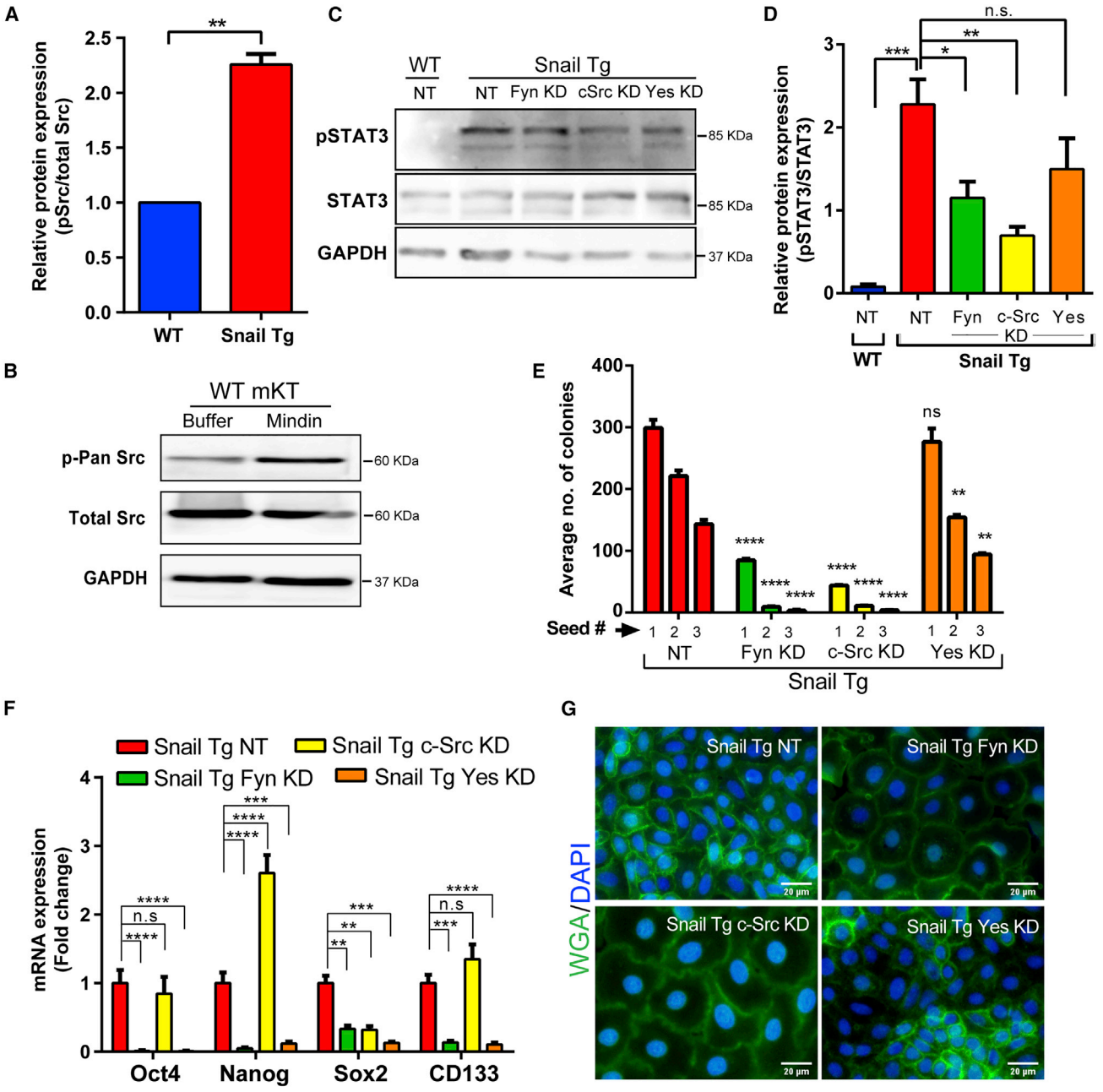

Figure 5. Src family of kinases mediate the Mindin-dependent activation of STAT3

(A) Quantification of phospho-pan-Src to total Src in WT and Snail Tg keratinocytes (n = 3).

(B) Western blot for phospho-pan-Src and total Src in WT keratinocytes treated with Mindin protein or its buffer control. GAPDH is the loading control (n = 3).

(C) Western blot for pSTAT3 and total STAT3 in WT and Snail Tg keratinocytes with non-targeting (NT) control or knockdown (KD) of *Fyn*, *c-Src*, or *Yes*. GAPDH is the loading control.

(D) Quantification of the western blots (n = 3) in (C).

(E) Number of colonies formed by Snail Tg keratinocytes knocked down for *Fyn*, *c-Src*, and *Yes* with NT as control (n = 3).

(F) mRNA expression of stem cell genes in the Snail Tg keratinocytes KD for *Fyn*, *c-Src*, or *Yes* with NT as control (n = 3).

(G) Immunofluorescence of WGA (green) and DAPI (blue) to determine NCR, which is reduced in Snail Tg cells with *Fyn* and *c-Src* KD compared with the Snail Tg NT and *Yes* KD cells. Scale bar, 20 μm. Data represent the mean ± SEM. p values were calculated using Student's t test (A), one-way ANOVA followed by Sidak's post hoc analysis (D), and two-way ANOVA followed by Tukey's post hoc analysis (E and F). *p < 0.05, **p < 0.01, ***p < 0.001, ****p < 0.0001, and n.s = not significant. See also Figure S5.

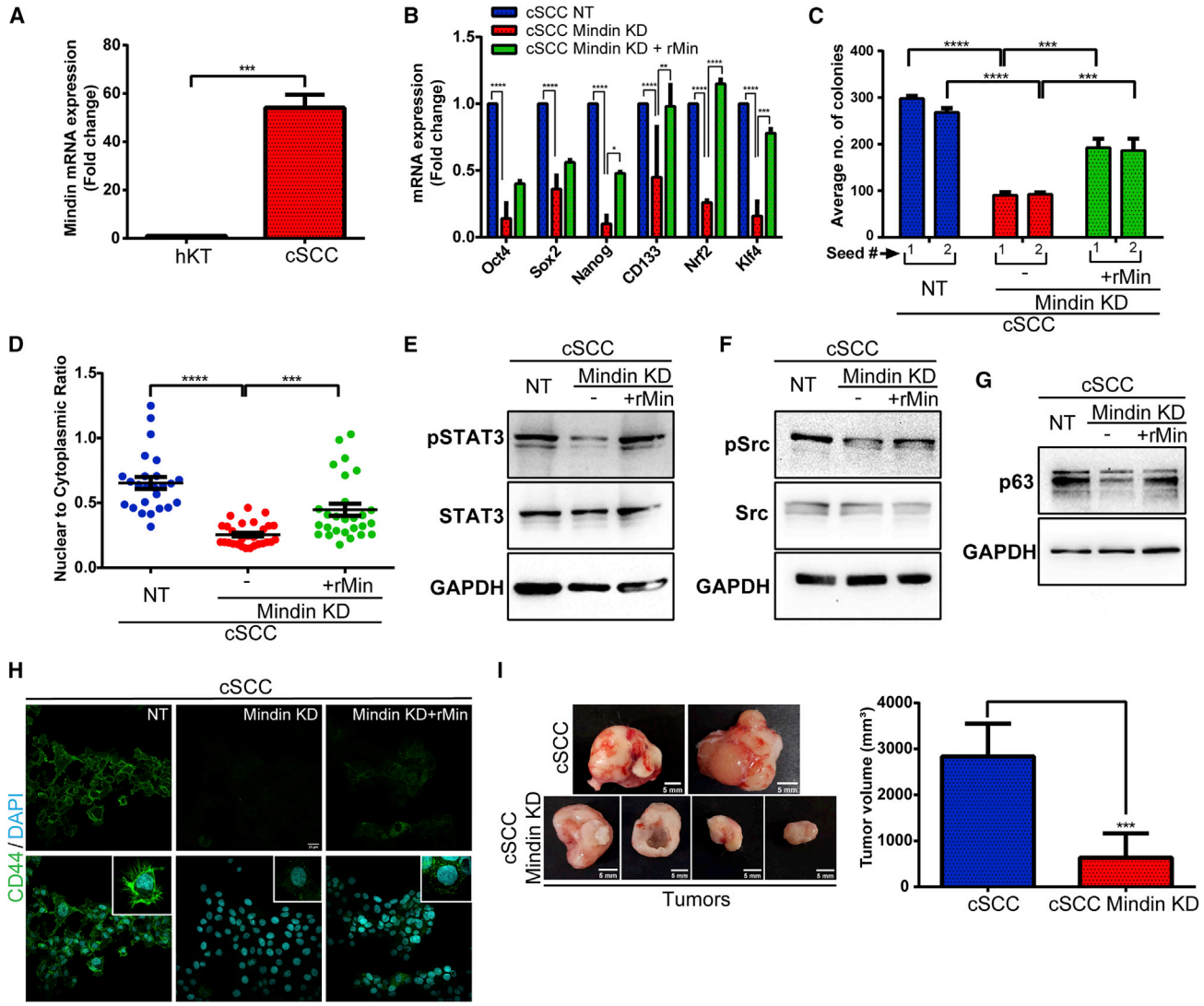

Figure 6. Mindin is required for the maintenance of stem/progenitor characteristics in cutaneous squamous cell carcinoma cells

(A) qPCR for Mindin RNA in patient-derived cutaneous squamous cell carcinoma (cSCC) cells compared with normal human keratinocytes (n = 3).

(B) mRNA expression of stem cell genes in cSCC NT control, cSCC Mindin KD, and cSCC Mindin KD treated + recombinant Mindin (rMin) (n = 3).

(C) Number of colonies formed by cSCC NT control cells, cSCC Mindin KD, and cSCC Mindin KD cells + rMin (n = 3).

(D) Nuclear to cytoplasmic ratio of cSCC NT control cells, cSCC Mindin KD, and cSCC Mindin KD cells treated with rMin (n = 3).

(E–G) Western blot analysis for pSTAT3 and total STAT3 (E), pSrc and total Src (F), and p63 (G) in cSCC NT control cells, cSCC Mindin KD, and cSCC Mindin KD cells treated with rMin.

(H) Immunofluorescence of cell surface marker CD44 in green on cSCC NT control cells, cSCC Mindin KD, and cSCC Mindin KD cells treated with rMin. Scale bar, 25 μm.

(I) Tumors formed by the cSCC cells (top) and cSCC Mindin KD cells (bottom) in the xenograft assay. Scale bar, 5 mm. Right panel is the tumor volume of cSCC and cSCC Mindin KD tumors (n = 5 for cSCC cells) (n = 10 for cSCC Mindin KD cells). Data represent the mean ± SEM. p values were calculated using Student's t test (A and I), two-way ANOVA followed by Dunnett's post hoc analysis (B), two-way ANOVA followed by Tukey's post hoc analysis (C), and one-way ANOVA followed by Tukey's post hoc analysis (D). *p < 0.05, **p < 0.01, ***p < 0.001, ****p < 0.0001. See also Figure S6.

keratinocytes, respectively (Figure 7B). This decrease in receptor localization at the plasma membrane is consistent with the endocytic activation of cell surface signaling molecules (Reinecke and Caplan, 2014). In line with this hypothesis, treatment of WT keratinocytes with increasing doses of Mindin resulted in increasing levels of pSTAT3 (Figures S7D and S7E). To test if the "leukocyte-specific" integrin CD11b had any role in epithelial cells, we blocked CD11b activity on keratinocytes with an inhibitory antibody and examined its impact on Mindin-induced stem/progenitor characteristics. Inhibition of CD11b blocked the ability of Mindin to induce the phosphorylation of STAT3 in WT keratinocytes (Figure 7C). In addition to this, inhibition of CD11b in human cSCC cells significantly reduced the levels of pSTAT3 compared with its isotype control (Figures 7D and 7E).

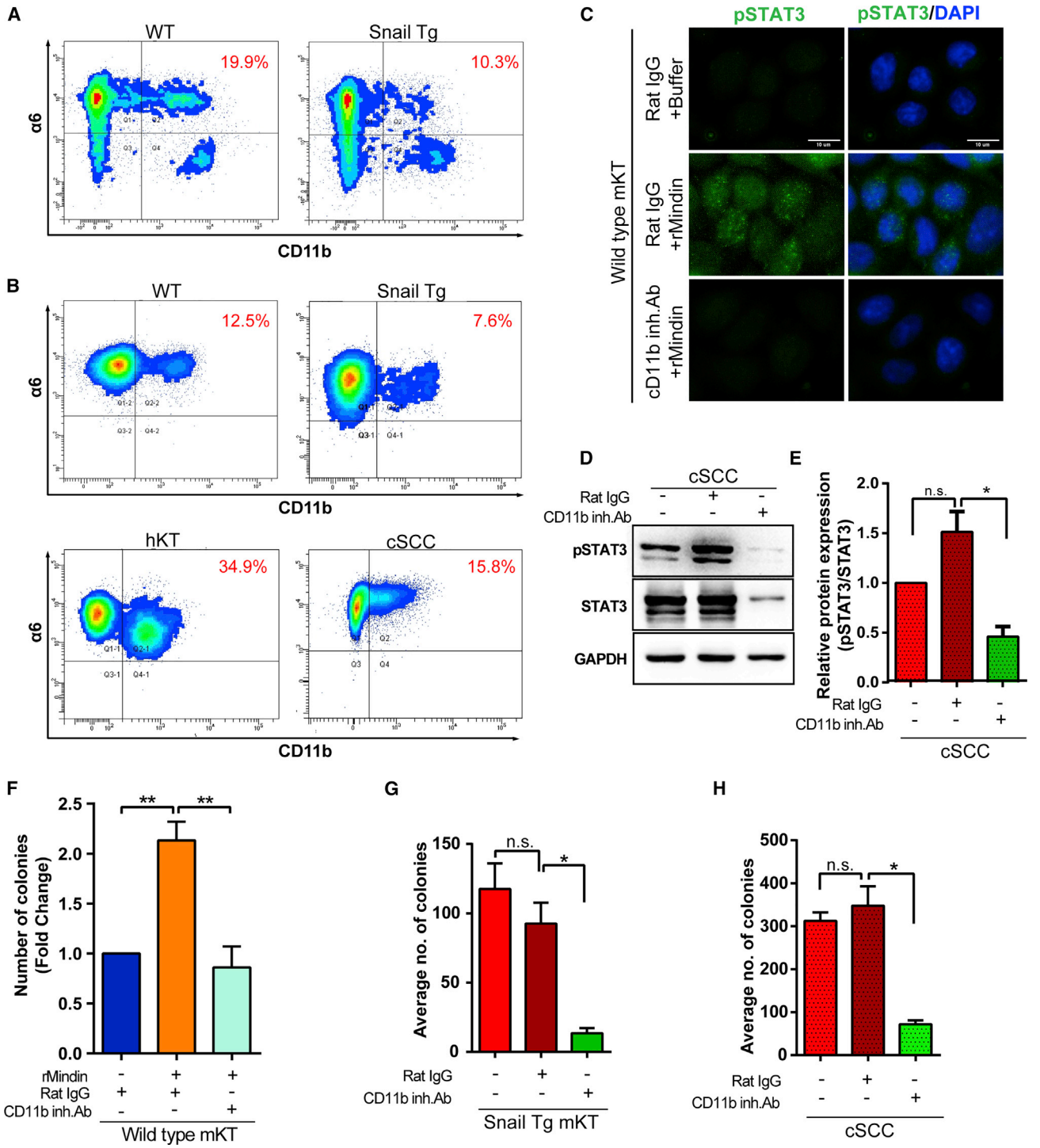

Figure 7. CD11b mediates Mindin signaling in Snail Tg keratinocytes and cSCC cells

(A) Flow cytometry analysis of CD11b membrane expression on WT and Snail Tg epidermal keratinocytes isolated from P9 mice. α6 is used to mark the epithelial cells.

(B) Flow cytometry analysis of CD11b membrane expression on WT and Snail Tg primary keratinocytes and hKT (human primary keratinocytes) and cSCC cells. α6 is used to mark the epithelial cells.

(C) Phosphorylated STAT3 (green) on WT keratinocytes and cells treated with either Rat IgG + Buffer, Rat IgG + rMindin, or CD11b inhibitory Ab + rMindin. Scale bar, 10 μm.

(D) Western blot for pSTAT3 and total STAT3 in cSCC cells treated with Rat IgG or CD11b inhibitory Ab. GAPDH is the loading control.

(legend continued on next page)

Furthermore, the CD11b inhibitory antibody abrogated the ability of Mindin to stimulate self-renewal (as measured by colony formation) in keratinocytes (Figure 7F). Similarly, there was nearly a complete ablation in colony-forming capacity when CD11b was blocked in Snail Tg keratinocytes (Figure 7G) or cSCC cells Figure 7H). Overall, these results reveal that the expression of the ''leukocyte-specific'' integrin CD11b on epidermal keratinocytes renders the cells responsive to Mindin and mediates its role in activating STAT3 to fortify the stemness of the cell.

DISCUSSION

The predominant model of Snail's contribution toward tumorigenesis in various carcinomas invokes its canonical function in promoting an EMT (Fan et al., 2012; Goossens et al., 2017; Smith et al., 2014; Yang et al., 2017; Zhu et al., 2012). Several studies have established Snail-mediated EMT in either transformed cell lines or cancerous cells that contain multiple genetic aberrations. Surprisingly, we observed that ectopically expressed Snail in primary epidermal keratinocytes results in the downregulation of E-cadherin RNA but not protein (Jamora et al., 2005). The notion of an EMT itself has undergone a renaissance due to the new appreciation of the spectrum of EMT characteristics (Grosse-Wilde et al., 2015; Pastushenko and Blanpain, 2019). Thus, the EMT program is no longer considered a binary process with a completely epithelial (E) or mesenchymal (M) phenotype (Grosse-Wilde et al., 2015; Kröger et al., 2019). Instead, an important intermediate, called the EM hybrid state, correlates with maximum stem cell characteristics (Bierie et al., 2017). However, computation of the EMT score using the transcriptome profile we generated with transgenic cells revealed a negative score (<0) in both WT and Snail Tg primary mouse keratinocytes, signifying their epithelial nature (Tan et al., 2014). This also suggests that Snail is not sufficient to induce EMT in primary cells and requires an additional drive to enter the EMT program that is present in transformed and cancer cell lines.

These results are consistent with studies that have implicated an EMT independent role for Snail in conferring cancer cells with stem cell-like traits (De Craene et al., 2014; Goossens et al., 2017; Ma et al., 2017; Mani et al., 2009; Zhou et al., 2014). Although this association is well-recognized, the mechanistic basis underlying this connection has thus far remained elusive. Our findings indicate that *Snail*-expressing keratinocytes utilize Mindin in an autocrine fashion to activate SFK-STAT3 signaling to promote stemness (Figure S7F). This study illustrates how carcinomas are a product of factors operating at multiple cellular levels ranging from transcription factors such as Snail to cytoplasmic proteins (i.e., SFK-STAT3) and extracellular components such as Mindin. Previously, we reported that one mechanism for STAT3 activation in epidermal keratinocytes of the *Snail* transgenic skin is the paracrine signaling of IL-17 released by activated resident γδT-cells (Du et al., 2010). Interestingly, we find that the increase in the number of active γδT-cells in the Snail Tg background is substantially reduced in the absence of Mindin (Figure S7G). This is in line with previous reports demonstrating the role of this protein in recruitment and activation of other immune cells (Jia et al., 2005). Together, these results suggest that Mindin regulates stemness in a multitiered fashion: it establishes an inflammatory microenvironment that reinforces the autocrine effect of Mindin to stimulate an intracellular signaling pathway that resists pro-differentiation cues. In addition, the defect in keratinocyte differentiation of Tg cells (Figures 1D and 1F) may be facilitated by epigenetic modifications since Snail has been previously reported to associate with the PRC2 complex to inhibit epithelial differentiation (Plikus et al., 2015).

Interestingly, in aggressive tumors, Snail and Mindin expression are increased along with the number of CSCs (Hojo et al., 2018; Kang et al., 2020; Zhao et al., 2020). Since we have demonstrated that secreted Mindin is both necessary and sufficient to maintain stemness, one would predict that many cells within its field would be stimulated to manifest stem cell characteristics. Why, then, are the number of CSCs within a tumor so few? Our data suggest that an additional factor(s) must be in place that puts a constraint on cells that are competent to respond to the stemness-maintaining activity of Mindin. While we observed that Snail is sufficient to induce Mindin expression in epithelial cells, it is not capable of upregulating its cognate receptor (CD11b) in cSCC cells. The elucidation of the regulatory control over CD11b expression in epithelial cancers would thus be an important avenue to pursue in the quest to target CSCs within the tumor mass. This has added importance as CD11b expression has been correlated with poor survival of patients with renal cancer (Boguslawska et al., 2016). An additional factor that may limit the number of cells that respond to Mindin is ECM-binding nature of the protein. Given that tumor cells themselves, along with cancer-associated fibroblasts, secrete excessive amounts of matrix protein, the ECM can substantially restrict diffusion of Mindin and thus limit the number of cells that are exposed to this matricellular protein.

Interestingly we found that the receptor for Mindin on epidermal keratinocytes is the integrin CD11b. This was unexpected as CD11b is widely considered a ''leukocyte-specific'' integrin. Additionally, we observed that engagement with Mindin leads to a reduction of CD11b at the plasma membrane. This was observed in Snail Tg keratinocytes and human SCC cells compared with their WT counterparts. One possible reason for this decrease is the internalization of CD11b upon ligand (Mindin) binding, indicative of its activation. In fact, this is the paradigm for the activation of Src and STAT3, which become activated on the endosomes following a stimulus (Reinecke and Caplan, 2014). Interestingly, Src kinases localized to the endosomal membrane have a functional role in tumor progression (Hikita et al., 2019). Likewise, in mouse embryonic stem cells and hematopoietic

(E) Quantification of pSTAT3 to total STAT3 in cSCC cells treated with Rat IgG and CD11b inhibitory Ab respectively (n = 2).
(F) Colonies formed by WT keratinocytes treated with Rat IgG + Buffer, Rat IgG + rMindin, or CD11b inhibitory Ab + rMindin (n = 4).
(G) Number of colonies formed by Snail Tg keratinocytes treated with Rat IgG and CD11b inhibitory Ab respectively (n = 5).
(H) Number of colonies formed by cSCC cells treated with Rat IgG and CD11b inhibitory Ab respectively (n = 2). Data represent the mean ± SEM. p values were calculated using one-way ANOVA followed by Sidak's post hoc analysis. *$p < 0.05$ and **$p < 0.01$ and n.s = not significant. See also Figure S7.

stem cells, STAT3 associated with the endosomes is required for the maintenance of the stemness of these cells (Sinha et al., 2013).

A notable observation made during the course of this study is that *Snail*-expressing keratinocytes exhibit an increase in both activated STAT3 as well as total STAT3 (Figure S3B). The reason for the latter could be a direct binding of Snail on the *STAT3* promoter, which has the canonical E-box sequence for Snail binding (Figure S7H). This would argue that even though Snail is classically considered a transcriptional repressor, it also has the ability to function as a transcriptional activator. This is supported by reports that Snail can transcriptionally upregulate *p15INK4b* (Hu et al., 2010), *MMP15* (Tao et al., 2011), and *Snail2* (Daisuke et al., 2006). This also explains why treatment of keratinocytes with Mindin only results in the upregulation of activated STAT3 without affecting the total amount of this protein (Figure 4G).

Given its role in maintaining stemness, STAT3 has been a focus in cancer therapy, and multiple drugs targeting this protein/pathway are currently in clinical trials. However, only a few STAT3 inhibitors are approved by the FDA (Beebe et al., 2018; Zou et al., 2020). One major limitation of targeting STAT3 is that since normal cells require this signaling protein for basic cellular physiology, inhibiting this protein would have many unintended side effects. Therefore, it becomes important to target specific upstream regulators of STAT3 that would allow other physiologically important STAT3-containing signaling pathways to remain operational. In this case, Mindin would be an attractive target as *Mindin* KO mice are viable and fertile and Mindin activates STAT3 in cancer cells. Additionally, in the *Mindin* KO mice, other physiological pathways utilizing STAT3 will still be intact. For instance, the *Snail* Tg/*Mindin* KO retains STAT3 activation in the basal keratinocytes of the epidermis where it is known to contribute to the proliferative potential of these cells (Figure 4). Finally, the activity of Mindin in both mouse and human squamous cell carcinoma of the skin suggests that this is a conserved process that would be an effective target for therapeutic intervention.

Limitations of the study

Given the importance of Mindin in our *in vitro* and *in vivo* systems, whether the amounts used in our studies match the concentrations found in the tumor microenvironment remains to be determined. It is also important to note that the markers used in our experiments are not exclusive to stem cells in the epidermis but also label transit amplifying cells, thus rendering our conclusions based on a mixed population of progenitor cells. Moreover, it has been observed that Mindin can exhibit both pro- and anti-tumor activities. This study is limited to squamous cell carcinoma of the skin wherein Mindin is tumorigenic, but the activity of Mindin may be cell type specific or modulated by additional signaling pathways/external factors within the tumor mass.

STAR★METHODS

Detailed methods are provided in the online version of this paper and include the following:

- KEY RESOURCES TABLE
- RESOURCE AVAILABILITY
  - Lead contact
  - Material availability
  - Data and code availability
- EXPERIMENTAL MODEL AND SUBJECT DETAILS
- METHOD DETAILS
  - Gene expression
  - Transcriptome and microarray data analysis
  - Analysis of EMT score of primary keratinocytes
  - Western blot analysis
  - Immunostaining and histology
  - Flow cytometry
  - Fluorescence-activated cell sorting
  - Calculation of nuclear to cytoplasmic ratio (NCR)
  - Colony formation assay
  - Xenograft assay
  - shRNA mediated knockdown
  - CRISPR/Cas9 mediated *Mindin* knockdown in cSCC cells
  - Plasmid engineering
  - Lentivirus production and transduction
  - Electron microscopy
- QUANTIFICATION AND STATISTICAL ANALYSIS

SUPPLEMENTAL INFORMATION

Supplemental information can be found online at https://doi.org/10.1016/j.celrep.2022.111390.

ACKNOWLEDGMENTS

The authors thank Satyajit Mayor, Maneesha Inamdar, Subhasri Ghosh, and Jamora lab members for their critical review of the work and insightful discussions, and Drs. Deepak Arya, Sangeetha Raajkamal, and Yogesh Chandra for technical assistance. This work was supported by core funds from inStem and grants from the Department of Biotechnology of the Government of India (BT/PR8738/AGR/36/770/2013) and (BT/PR32539/BRB/10/1814/2019), the National Institute of Arthritis and Musculoskeletal and Skin Diseases (NIAMS), NIH (5R01AR053185-03); the American Cancer Society (15457-RSG-08-164-01-DDC), and by a Hellman Faculty Fellowship to C.J.; Work in the S.K. lab is supported by NCBS-TIFR planned funds. R.K.Z. was supported by a Junior Research Fellowship from the DBT (DBT/JRF/13/AL/486). R.D. was supported by DBT-RA Fellowship. Animal studies were partially supported by the National Mouse Research Resource (NaMoR) grant BT/PR5981/MED/31/181/2012; 2013–2016; 2018 and 102/IFD/SAN/5003/2017–2018 from the DBT. We thank the staff of the BLiSC Animal Care and Resource Center for assistance with animal husbandry, the BLiSC Central Imaging and Flow Cytometry facility for help with image acquisition, and the BLiSC Electron Microscopy facility for ultrastructural analysis of the skin, and Dr. Benjamin D. Yu (University of California, San Diego) for the gift of the A388 cell line.

AUTHOR CONTRIBUTIONS

Conceptualization, K.B. and C.J.; methodology, K.B. and C.J.; investigation, K.B., B.D., S.K., R.K.Z., R.S., T.M., R.D., and A.G.; validation, K.B., B.D., G.K., A.H., J.A., S.P.S., and S.K.; formal analysis, R.D., J.S., and P.K.; resources, C.J., S.K., R.S., A.G., and Y.W.H., writing – original draft, K.B. and C.J.; funding acquisition, C.J. and S.K.; supervision, C.J. and S.K.

DECLARATION OF INTERESTS

The authors declare no competing interests.

Received: January 6, 2022
Revised: June 11, 2022
Accepted: August 30, 2022
Published: September 20, 2022

REFERENCES

Alday-Parejo, B., Stupp, R., and Rüegg, C. (2019). Are integrins still practicable targets for anti-cancer therapy? Cancers *11*.

Anders, S., Pyl, P.T., and Huber, W. (2015). HTSeq-A Python framework to work with high-throughput sequencing data. Bioinformatics *31*, 166–169.

Beck, B., Lapouge, G., Rorive, S., Drogat, B., Desaedelaere, K., Delafaille, S., Dubois, C., Salmon, I., Willekens, K., Marine, J.C., and Blanpain, C. (2015). Different levels of Twist1 regulate skin tumor initiation, stemness, and progression. Cell Stem Cell *16*, 67–79.

Beebe, J.D., Liu, J.Y., and Zhang, J.T. (2018). Two decades of research in discovery of anticancer drugs targeting STAT3, how close are we? Pharmacol. Ther. *191*, 74–91.

Bierie, B., Pierce, S.E., Kroeger, C., Stover, D.G., Pattabiraman, D.R., Thiru, P., Liu Donaher, J., Reinhardt, F., Chaffer, C.L., Keckesova, Z., and Weinberg, R.A. (2017). Integrin-β4 identifies cancer stem cell-enriched populations of partially mesenchymal carcinoma cells. Proc. Natl. Acad. Sci. USA *114*, E2337–E2346.

Bikle, D.D., Xie, Z., and Tu, C.L. (2012). Calcium regulation of keratinocyte differentiation. Expert Rev. Endocrinol. Metab. *7*, 461–472.

Blanpain, C., and Fuchs, E. (2006). Epidermal stem cells of the skin. Annu. Rev. Cell Dev. Biol. *22*, 339–373.

Blanpain, C., and Fuchs, E. (2007). P63: revving up epithelial stem-cell potential. Nat. Cell Biol. *9*, 731–733.

Boguslawska, J., Kedzierska, H., Poplawski, P., Rybicka, B., Tanski, Z., and Piekielko-Witkowska, A. (2016). Expression of genes involved in cellular adhesion and extracellular matrix remodeling correlates with poor survival of patients with renal cancer. J. Urol. *195*, 1892–1902.

Bowman, T., Garcia, R., Turkson, J., and Jove, R. (2000). STATs in Oncogenesis, pp. 2474–2488.

Conway, K., Morgan, D., Phillips, K.K., Yuspa, S.H., and Weissman, B.E. (1992). Tumorigenic Suppression of a Human Cutaneous Squamous Cell Carcinoma Cell Line in the Nude Mouse Skin Graft Assay 1.

De Craene, B., Denecker, G., Vermassen, P., Taminau, J., Mauch, C., Derore, A., Jonkers, J., Fuchs, E., and Berx, G. (2014). Epidermal Snail expression drives skin cancer initiation and progression through enhanced cytoprotection, epidermal stem/progenitor cell expansion and enhanced metastatic potential. Cell Death Differ. *21*, 310–320.

Sakai, D., Suzuki, T., Osumi, N., and Wakamatsu, Y. (2006). Cooperative action of Sox9, Snail2 and PKA signaling in early neural crest development. Development *133*, 1323–1333.

Du, F., Nakamura, Y., Tan, T.L., Lee, P., Lee, R., Yu, B., and Jamora, C. (2010). Expression of snail in epidermal keratinocytes promotes cutaneous inflammation and hyperplasia conducive to tumor formation. Cancer Res. *70*, 10080–10089.

Fan, F., Samuel, S., Evans, K.W., Lu, J., Xia, L., Zhou, Y., Sceusi, E., Tozzi, F., Ye, X.C., Mani, S.A., and Ellis, L.M. (2012). Overexpression of Snail induces epithelial–mesenchymal transition and a cancer stem cell–like phenotype in human colorectal cancer cells. Cancer Med. *1*, 5–16.

Franken, N.A.P., Rodermond, H.M., Stap, J., Haveman, J., and van Bree, C. (2006). Clonogenic assay of cells in vitro. Nat. Protoc. *1*, 2315–2319.

Fuchs, E. (2008). Skin stem cells: rising to the surface. J. Cell Biol. *180*, 273–284.

Galoczova, M., Coates, P., and Vojtesek, B. (2018). STAT3, stem cells, cancer stem cells and p63. Cell. Mol. Biol. Lett. *23*, 12.

Ganguly, K.K., Pal, S., Moulik, S., and Chatterjee, A. (2013). Integrins and metastasis. Cell Adh. Migr. *7*, 251–261.

Gingold, J.A., Fidalgo, M., Guallar, D., Lau, Z., Sun, Z., Zhou, H., Faiola, F., Huang, X., Lee, D.F., Waghray, A., et al. (2014). A genome-wide RNAi screen identifies opposing functions of Snai1 and Snai2 on the Nanog dependency in reprogramming. Mol. Cell *56*, 140–152.

Goossens, S., Vandamme, N., Van Vlierberghe, P., and Berx, G. (2017). EMT transcription factors in cancer development re-evaluated: beyond EMT and MET. Biochim. Biophys. Acta. Rev. Cancer *1868*, 584–591.

Grandis, J.R., Drenning, S.D., Chakraborty, A., Zhou, M.Y., Zeng, Q., Pitt, A.S., and Tweardy, D.J. (1998). Requirement of Stat3 but not Stat1 activation for epidermal growth factor receptor- mediated cell growth in vitro. J. Clin. Invest. *102*, 1385–1392.

Grosse-Wilde, A., Fouquier d'Hérouël, A., McIntosh, E., Ertaylan, G., Skupin, A., Kuestner, R.E., del Sol, A., Walters, K.-A., and Huang, S. (2015). Stemness of the hybrid epithelial/mesenchymal state in breast cancer and its association with poor survival. PLoS One *10*, e0126522.

Hikita, T., Kuwahara, A., Watanabe, R., Miyata, M., and Oneyama, C. (2019). Src in endosomal membranes promotes exosome secretion and tumor progression. Sci. Rep. *9*, 3265–3314.

Hojo, N., Huisken, A.L., Wang, H., Chirshev, E., Kim, N.S., Nguyen, S.M., Campos, H., Glackin, C.A., Ioffe, Y.J., and Unternaehrer, J.J. (2018). Snail knockdown reverses stemness and inhibits tumour growth in ovarian cancer. Sci. Rep. *8*, 8704–8710.

Hu, C.T., Chang, T.Y., Cheng, C.C., Liu, C.S., Wu, J.R., Li, M.C., and Wu, W.S. (2010). Snail associates with EGR-1 and SP-1 to upregulate transcriptional activation of p15INK4b. FEBS J. *277*, 1202–1218.

Huang, D.W., Sherman, B.T., and Lempicki, R.A. (2009). Systematic and integrative analysis of large gene lists using DAVID bioinformatics resources. Nat. Protoc. *4*, 44–57.

Jamora, C., Lee, P., Kocieniewski, P., Azhar, M., Hosokawa, R., Chai, Y., and Fuchs, E. (2005). A signaling pathway involving TGF-β2 and snail in hair follicle morphogenesis. PLoS Biol. *3*, e11.

Jia, W., Li, H., and He, Y.W. (2005). The extracellular matrix protein mindin serves as an integrin ligand and is critical for inflammatory cell recruitment. Blood *106*, 3854–3859.

Jin, C., Lin, J.R., Ma, L., Song, Y., Shi, Y.X., Jiang, P., Dong, Y., and Li, X.S. (2017). Elevated spondin-2 expression correlates with progression and prognosis in gastric cancer. Oncotarget *8*, 10416–10424.

Jung, H.Y., and Yang, J. (2015). Unraveling the TWIST between EMT and cancer stemness. Cell Stem Cell *16*, 1–2.

Kang, H.-G., Kim, W.-J., Noh, M.-G., Chun, K.-H., and Kim, S.-J. (2020). SPON2 is upregulated through Notch signaling pathway and promotes tumor progression in gastric cancer. Cancers *12*, 1439.

Kim, D., Paggi, J.M., Park, C., Bennett, C., and Salzberg, S.L. (2019). Graph-based genome alignment and genotyping with HISAT2 and HISAT-genotype. Nat. Biotechnol. *37*, 907–915.

Koster, M.I., Kim, S., and Roop, D.R. (2005). P63 deficiency: a failure of lineage commitment or stem cell maintenance? J. Investig. Dermatol. Symp. Proc. *10*, 118–123.

Krebsbach, P.H., and Villa-Diaz, L.G. (2017). The role of integrin α6 (CD49f) in stem cells: more than a conserved biomarker. Stem Cells Dev. *26*, 1090–1099.

Kröger, C., Afeyan, A., Mraz, J., Eaton, E.N., Reinhardt, F., Khodor, Y.L., Thiru, P., Bierie, B., Ye, X., Burge, C.B., and Weinberg, R.A. (2019). Acquisition of a hybrid E/M state is essential for tumorigenicity of basal breast cancer cells. Proc. Natl. Acad. Sci. USA *116*, 7353–7362.

Li, Y., Kong, D., Ahmad, A., Bao, B., and Sarkar, F.H. (2013). Pancreatic cancer stem cells: Emerging target for designing novel therapy. Cancer Lett. *338*, 94–100.

Li, Y., Wang, Z., Ajani, J.A., and Song, S. (2021). Drug resistance and Cancer stem cells. Cell Commun. Signal. *19*, 1–11.

Love, M.I., Huber, W., and Anders, S. (2014). Moderated estimation of fold change and dispersion for RNA-seq data with DESeq2. Genome Biol. *15*, 550.

Lucarelli, G., Rutigliano, M., Bettocchi, C., Palazzo, S., Vavallo, A., Galleggiante, V., Trabucco, S., Di Clemente, D., Selvaggi, F.P., Battaglia, M., and Ditonno, P. (2013). Spondin-2, a secreted extracellular matrix protein, is a novel diagnostic biomarker for prostate cancer. J. Urol. *190*, 2271–2277.

Ma, S.Y., Park, J.H., Jung, H., Ha, S.M., Kim, Y., Park, D.H., Lee, D.H., Lee, S., Chu, I.H., Jung, S.Y., et al. (2017). Snail maintains metastatic potential, cancer stemlike properties, and chemoresistance in mesenchymal mouse breast cancer TUBO-P2J cells. Oncol. Rep. *38*, 1867–1876.

Mani, S.a., Guo, W., Liao, M.J., Eaton, E.N., Ayyanan, A., Zhou, A.Y., Brooks, M., Reinhard, F., Zhang, C.C., Shipitsin, M., et al. (2008). Epithelial-mesenchymal transition generates cells which have stem cell properties. Cell *133*, 704–715.

Matsui, W.H. (2016). Cancer stem cell signaling pathways. Medicine *95*, S8–S19.

Meng, F., and Lowell, C.A. (1998). A β1 integrin signaling pathway involving Src-family kinases, Cbl and PI-3 kinase is required for macrophage spreading and migration. EMBO J. *17*, 4391–4403.

Mistry, D.S., Chen, Y., Wang, Y., Zhang, K., and Sen, G.L. (2014). SNAI2 controls the undifferentiated state of human epidermal progenitor cells. Stem Cell. *32*, 3209–3218.

Murray, S.A., and Gridley, T. (2006). Snail1 gene function during early embryo patterning in mice. Cell Cycle *5*, 2566–2570.

Nakasaki, M., Hwang, Y., Xie, Y., Kataria, S., Gund, R., Hajam, E.Y., Samuel, R., George, R., Danda, D., Mj, P., et al. (2015). The matrix protein Fibulin-5 is at the interface of tissue stiffness and inflammation in fibrosis. Nat. Commun. *6*, 8574.

Ni, H., Ni, T., Feng, J., Bian, T., Liu, Y., and Zhang, J. (2019). Spondin-2 is a novel diagnostic biomarker for laryngeal squamous cell carcinoma. Pathol. Res. Pract. *215*, 286–291.

Nowak, J.A., and Fuchs, E. (2009). Isolation and culture of epithelial stem cells. Methods Mol. Biol. *482*, 215–232.

Pastushenko, I., and Blanpain, C. (2019). EMT transition states during tumor progression and metastasis. Trends Cell Biol. *29*, 212–226.

Phi, L.T.H., Sari, I.N., Yang, Y.G., Lee, S.H., Jun, N., Kim, K.S., Lee, Y.K., and Kwon, H.Y. (2018). Cancer stem cells (CSCs) in drug resistance and their therapeutic implications in cancer treatment. Stem Cells Int., 5416923.

Pincha, N., Hajam, E.Y., Badarinath, K., Batta, S.P.R., Masudi, T., Dey, R., Andreasen, P., Kawakami, T., Samuel, R., George, R., et al. (2018). PAI1 mediates fibroblast-mast cell interactions in skin fibrosis. J. Clin. Invest. *128*, 1807–1819. https://doi.org/10.1172/JCI99088.

Plaks, V., Kong, N., and Werb, Z. (2015). The cancer stem cell niche: how essential is the niche in regulating stemness of tumor cells? Cell Stem Cell *16*, 225–238.

Plikus, M.V., Guerrero-Juarez, C.F., Treffeisen, E., and Gay, D.L. (2015). Epigenetic control of skin and hair regeneration after wounding. Exp. Dermatol. *24*, 167–170.

Rana, I., Kataria, S., Tan, T.L., Hajam, E.Y., Kashyap, D.K., Saha, D., Ajnabi, J., Paul, S., Jayappa, S., Ananthan, A.S., et al. (2022). Mindin is essential for cutaneous fibrogenesis in a new mouse model of systemic sclerosis. Preprint at bioRxiv. https://doi.org/10.1101/2022.01.26.477822.

Raz, R., Lee, C.-K., Cannizzaro, L.A., D'eustachio, P., and Levy, D.E. (1999). Essential Role of STAT3 for Embryonic Stem Cell Pluripotency (Leukemia Inhibitory Factorcytokine signalingJAK-STAT Pathwayembryonic Stem Cell Differentiation.

Rébé, C., Végran, F., Berger, H., Ghiringhelli, F., Georges, C., Leclerc, F., Médecine, F.D., and Bourgogne, U.D. (2013). A key factor in tumor immunoescape STAT3 activation, pp. 1–10.

Reinecke, J., and Caplan, S. (2014). Endocytosis and the Src family of non-receptor tyrosine kinases. Biomol. Concepts *5*, 143–155.

Saed, G.M., Fletcher, N.M., Diamond, M.P., Morris, R.T., Gomez-Lopez, N., and Memaj, I. (2018). Novel expression of CD11b in epithelial ovarian cancer: potential therapeutic target. Gynecol. Oncol. *148*, 567–575.

Scheel, C., Eaton, E.N., Li, S.H.J., Chaffer, C.L., Reinhardt, F., Kah, K.J., Bell, G., Guo, W., Rubin, J., Richardson, A.L., and Weinberg, R.A. (2011). Paracrine and autocrine signals induce and maintain mesenchymal and stem cell states in the breast. Cell *145*, 926–940.

Schindelin, J., Arganda-Carreras, I., Frise, E., Kaynig, V., Longair, M., Pietzsch, T., Preibisch, S., Rueden, C., Saalfeld, S., Schmid, B., et al. (2012). Fiji - an Open Source platform for biological image analysis. Nat. Methods *9*, 676–682.

Schmitges, F.W., Radovani, E., Najafabadi, H.S., Barazandeh, M., Campitelli, L.F., Yin, Y., Jolma, A., Zhong, G., Guo, H., Kanagalingam, T., et al. (2016). Multiparameter functional diversity of human C2H2 zinc finger proteins. Genome Res. *26*, 1742–1752.

Schober, M., and Fuchs, E. (2011). Tumor-initiating stem cells of squamous cell carcinomas and their control by TGF-β and integrin/focal adhesion kinase (FAK) signaling. Proc. Natl. Acad. Sci. USA *108*, 10544–10549.

Simon, I., Liu, Y., Krall, K.L., Urban, N., Wolfert, R.L., Kim, N.W., and McIntosh, M.W. (2007). Evaluation of the novel serum markers B7-H4, Spondin 2, and DcR3 for diagnosis and early detection of ovarian cancer. Gynecol. Oncol. *106*, 112–118.

Sinha, A., Khadilkar, R.J., S, V.K., RoyChowdhury Sinha, A., and Inamdar, M.S. (2013). Conserved Regulation of the JAK/STAT Pathway by the Endosomal Protein Asrij Maintains Stem Cell Potency.

Smith, B.N., Burton, L.J., Henderson, V., Randle, D.D., Morton, D.J., Smith, B.A., Taliaferro-Smith, L., Nagappan, P., Yates, C., Zayzafoon, M., et al. (2014). Snail promotes epithelial mesenchymal transition in breast cancer cells in Part via activation of nuclear ERK2. PLoS One *9*, e104987.

Sun, H.R., Wang, S., Yan, S.C., Zhang, Y., Nelson, P.J., Jia, H.L., Qin, L.X., and Dong, Q.Z. (2019). Therapeutic strategies targeting cancer stem cells and their microenvironment. Front. Oncol. *9*, 1104.

Tan, T.Z., Miow, Q.H., Miki, Y., Noda, T., Mori, S., Huang, R.Y.J., and Thiery, J.P. (2014). Epithelial-mesenchymal transition spectrum quantification and its efficacy in deciphering survival and drug responses of cancer patients. EMBO Mol. Med. *6*, 1279–1293.

Tao, G., Levay, A.K., Gridley, T., and Lincoln, J. (2011). Mmp15 is a direct target of Snai1 during endothelial to mesenchymal transformation and endocardial cushion development. Dev. Biol. *359*, 209–221.

Wang, H., and Unternaehrer, J.J. (2019). Epithelial-mesenchymal transition and cancer stem cells: at the crossroads of differentiation and dedifferentiation. Dev. Dyn. *248*, 10–20.

Wu, J., Gao, W., Tang, Q., Yu, Y., You, W., Wu, Z., Fan, Y., Zhang, L., Wu, C., Han, G., et al. (2021). M2 macrophage–derived Exosomes facilitate HCC metastasis by transferring αMβ2 integrin to tumor cells. Hepatology *73*, 1365–1380.

Xia, H., Li, X., Gao, W., Fu, X., Fang, R.H., Zhang, L., and Zhang, K. (2018). Tissue repair and regeneration with endogenous stem cells. Nat. Rev. Mater. *3*, 174–193.

Xue, Z.-H., Zhao, C.-Q., Chua, G.-L., Tan, S.-W., Tang, X.-Y., Wong, S.-C., and Tan, S.-M. (2010). Integrin α M β 2 clustering triggers phosphorylation and activation of protein kinase Cδ that regulates transcription factor Foxp1 expression in monocytes. J. Immunol. *184*, 3697–3709.

Yadavalli, S., Jayaram, S., Manda, S.S., Madugundu, A.K., Nayakanti, D.S., Tan, T.Z., Bhat, R., Rangarajan, A., Chatterjee, A., Gowda, H., et al. (2017). Data-driven discovery of Extravasation pathway in Circulating tumor cells. Sci. Rep. *7*, 43710.

Yang, S.W., Zhang, Z.G., Hao, Y.X., Zhao, Y.L., Qian, F., Shi, Y., Li, P.A., Liu, C.Y., and Yu, P.W. (2017). HIF-1α induces the epithelial-mesenchymal transition in gastric cancer stem cells through the Snail pathway. Oncotarget *8*, 9535–9545.

Yang, L., Shi, P., Zhao, G., Xu, J., Peng, W., Zhang, J., Zhang, G., Wang, X., Dong, Z., Chen, F., and Cui, H. (2020). Targeting cancer stem cell pathways for cancer therapy. Signal Transduct. Target. Ther. *5*, 8–35.

Ye, F., Zhong, X., Qiu, Y., Yang, L., Wei, B., Zhang, Z., and Bu, H. (2017). CD49f can act as a biomarker for local or distant recurrence in breast cancer. J. Breast Cancer *20*, 142–149.

Yu, Y., Ramena, G., and Elble, R.C. (2012). The role of cancer stem cells in relapse of solid tumors. Front. Biosci. *4*, 1528–1541.

Yuan, X., Bian, T., Liu, J., Ke, H., Feng, J., Zhang, Q., Qian, L., Li, X., Liu, Y., and Zhang, J. (2017). Spondin2 is a new prognostic biomarker for lung adenocarcinoma. Oncotarget *8*, 59324–59332.

Zhang, X., Yue, P., Page, B.D.G., Li, T., Zhao, W., Namanja, A.T., Paladino, D., Zhao, J., Chen, Y., Gunning, P.T., and Turkson, J. (2012). Orally bioavailable small-molecule inhibitor of transcription factor Stat3 regresses human breast and lung cancer xenografts. Proc. Natl. Acad. Sci. USA *109*, 9623–9628.

Zhang, Q., Wang, X.Q., Wang, J., Cui, S.J., Lou, X.M., Yan, B., Qiao, J., Jiang, Y.H., Zhang, L.J., Yang, P.Y., and Liu, F. (2015). Upregulation of spondin-2 predicts poor survival of colorectal carcinoma patients. Oncotarget *6*, 15095–15110.

Zhao, G., Kim, K.Y., Zheng, Z., Oh, Y., Yoo, D.S., Lee, M.E., Chung, K.Y., Roh, M.R., and Jin, Z. (2020). AXIN2 and SNAIL expression predict the risk of recurrence in cutaneous squamous cell carcinoma after Mohs micrographic surgery. Oncol. Lett. *19*, 2133–2140.

Zheng, M., Jiang, Y.P., Chen, W., Li, K.d., Liu, X., Gao, S.Y., Feng, H., Wang, S.S., Jiang, J., Ma, X.R., et al. (2015). Snail and slug collaborate on EMT and tumor metastasis through mir-101-mediated EZH2 axis in oral tongue squamous cell carcinoma. Oncotarget *6*, 6797–6810.

Zhou, W., Zhao, M., Wang, X., Schilling, R.F., Zhou, S., Qiu, H.Y., Xie, N.H., Liu, M.Q., Dong, H.S., Yao, Z.Z., and Cai, T. (2014). Snail contributes to the maintenance of stem cell-like phenotype cells in human pancreatic cancer. PLoS One *9*, e113736.

Zhu, L.F., Hu, Y., Yang, C.C., Xu, X.H., Ning, T.Y., Wang, Z.L., Ye, J.H., and Liu, L.K. (2012). Snail overexpression induces an epithelial to mesenchymal transition and cancer stem cell-like properties in SCC9 cells. Lab. Invest. *92*, 744–752.

Zou, S., Tong, Q., Liu, B., Huang, W., Tian, Y., and Fu, X. (2020). Targeting stat3 in cancer immunotherapy. Mol. Cancer *19*, 145–219.

STAR★METHODS

KEY RESOURCES TABLE

REAGENT or RESOURCE	SOURCE	IDENTIFIER
Antibodies		
Total STAT3	CST	Cat # 4904; RRID:AB_331269
Phospho STAT3	CST	Cat # 9145; RRID:AB_2491009
p63	Abcam	Cat # ab97865; RRID:AB_10680707
GAPDH	CST	Cat # 5174; RRID:AB_10622025
Tubulin	Sigma-Aldrich	Cat # T5326; RRID:AB_532292
WGA	Invitrogen	Cat # W32466
DAPI	Sigma	Cat # MBD0015
Keratin 5	Jamora lab generated	N/A
CD49f	BD Biosciences	Cat # 561894; RRID:AB_10897164
CD44	BD Biosciences	Cat # 550538; RRID:AB_393732
Mindin	Santa Cruz	Cat # SC49050; RRID:AB_2270943
Total Src	CST	Cat # 2123; RRID:AB_2106047
Phospho Src	CST	Cat # 6943; RRID:AB_10013641
CD11b	eBioscience	Cat # 14-0112-82; RRID:AB_467108
CD11b APC-eFluor 780	eBioscience	Cat # 47-0112-82; RRID:AB_1603193
Chemicals, peptides, and recombinant proteins		
STAT3 inhibitor	Millipore	Cat # 573132
Src inhibitor	Millipore	Cat # 567805
Matrigel	BD Biosciences	Cat # 354277
Mindin	This paper	N/A
PowerUp SYBR Green Master Mix	Applied Biosystems	Cat # A25742
Collagen	Biolix Technologies LLP	Cat # 08-115
Deposited data		
RNA seq- RAW data	This paper	PRJNA850106
SNAI2 ChIP-seq dataset	Mistry et al., 2014	GSE55421
SNAI1 ChIP-seq dataset	Schmitges et al., 2016	GSE76496
Experimental models: Cell lines		
A388	Dr. Benjamin D. Yu (University of California, San Diego)	N/A
Human Epidermal Keratinocytes (Indian Origin)	Lonza	#192907
293T	ATCC	# CRL-3216
Experimental models: Organisms/strains		
Mouse: C57Bl6	The Jackson Laboratory	000664
Mouse: NSG	The Jackson Laboratory	005557
Mouse: K14-Snail Tg	Jamora et al., 2005	N/A
Mouse: Mindin KO	Prof. You-Wen He, Duke University Medical Center - Jia et al., 2005	N/A
Oligonucleotides		
qPCR primers for various genes	This paper	Table S1
shRNA constructs	This paper	Table S2
Recombinant DNA		
p-lentiCRISPR - EGFP sgRNA 1	Addgene	Cat # 51760
Plasmid - psPAX2	Addgene	Cat # 12260
Plasmid pMD2.G	Addgene	Cat # 12259

(*Continued on next page*)

Continued

REAGENT or RESOURCE	SOURCE	IDENTIFIER
Software and algorithms		
ImageJ (Fiji)	Schindelin et al., 2012	https://fiji.sc/
Prism version 6.0	GraphPad	https://www.graphpad.cpm/

RESOURCE AVAILABILITY

Lead contact

Further information and requests for resources and reagents should be directed to and will be fulfilled by the lead contact, Colin Jamora (colinj@instem.res.in).

Material availability

This study did not generate new unique reagents.

Data and code availability

- The data generated in this study are deposited in SRA with accession number PRJNA850106, https://www.ncbi.nlm.nih.gov/bioproject/PRJNA850106/.
- No new software code was developed for this study.
- Any additional information required to reanalyze the data reported in this paper is available from the lead contact upon request.

EXPERIMENTAL MODEL AND SUBJECT DETAILS

C57Bl6 and NSG mice (noted in the Key Resource Table) were obtained from The Jackson Laboratory (Bar Harbor, Maine) and *Mindin* KO mice was from You-Wen He (Department of Immunology, Duke University Medical University Medical Center) The *K14-Snail* Tg mouse was developed as described earlier (Jamora et al., 2005). The *K14-Snail Tg/Mindin* KO mouse was generated by breeding the *Mindin KO* and *K14-Snail Tg* mice. All mice were maintained and bred at the BLiSC Animal Care and Resource Center under specific pathogen–free conditions. Mice were sacrificed between P7 and P9 (neonatal) and skin samples were collected for RNA, protein and OCT or paraffin embedding as required. Mice of the both sexes were used in most experiments, with littermate controls. For all experiments involving NSG mice, 8 weeks old males were used. All animal work was approved by the Institutional Animal Ethics Committee in the CJ lab (INS-IAE-2019/06[R1]) and SK lab (NCBS-IAC-2017/05[N]). Experiments on mice followed the norms specified by the Committee for the Purpose of Control and Supervision of Experiments on Animals (Government of India). All experimental work was approved by the Institutional Biosafety Committees of both inStem and NCBS.

Primary epidermal keratinocytes were isolated and cultured as described previously in (Nowak and Fuchs, 2009). The keratinocytes were grown in low calcium (50uM) E-media for most of the assays and for the differentiation assay by calcium switch, E-media containing 1.2mM calcium was used and cultured for 24,48 and 72 h. Treatment with recombinant Mindin protein and conditioned media was done for 24 h. Human cutaneous squamous cell carcinoma cell line, A388 provided by Benjamin D. Yu (University of California, San Diego) was cultured in DMEM high glucose media with 10% FBS. All cells were processed as required for RNA and protein extraction or staining.

METHOD DETAILS

Gene expression

Total RNA was isolated from skin and epidermal biopsies or keratinocytes (either proliferating or differentiated) using TRIzol Reagent or RNAiso Plus (Thermo Fisher Scientific, Takara). 1-2ug of RNA was used to synthesise cDNA using Superscript III or PrimeScript kit (Thermo Fisher Scientific, Takara). Quantitative PCR (qPCR) was done with cDNA equivalent to approximately 100ng of RNA using the Sso Fast 2x master mix (BioRad) in a Bio-Rad CFX384 machine. Actin or GAPDH expression was used as a reference for normalization. The primer sequences used are listed in Table S1.

Transcriptome and microarray data analysis

For studying the transcriptome, total RNA was isolated from 6 samples (3 each from WT and Snail Tg keratinocyte samples). The RNA sample QC, NGS library (Illumina) preparation, and sequencing steps were outsourced to a commercial facility. We had received approximately 45–55 million and 80–90 million 150bp paired end reads from WT and Snail Tg samples, respectively. Analysis of the data was done in-house after receiving the raw sequencing reads. For the analysis, established analysis pipeline was used to study our RNA sequencing data. The quality of the raw sequencing reads was checked through FASTQC tool

[https://www.bioinformatics.babraham.ac.uk/projects/fastqc/]. The low-quality reads toward both ends were trimmed using "FASTX-TRIMMER" using the parameters as "-f 11 -L 140" [http://hannonlab.cshl.edu/fastx_toolkit/index.html]. The trimmed reads (130bp*2) were then aligned to mouse reference genome (mm10, UCSC version) using "HISAT2" (Kim et al., 2019). The "SAM" outputs were converted to "BAM" files, followed by sorting using "Samtools". Respective "BAM" files were used to generate "Count" matrix using "HTSeq-count" (Anders et al., 2015). The count matrix was used to calculate differentially expressed genes using "DESeq2" R package (Love et al., 2014). We found 1113 genes to be significantly differentially expressed in pairwise comparison (Adj p values <0.05). These genes were used for Gene Ontology (GO) enrichment analysis using "DAVID"(Huang et al., 2009).

Gene expression patterns of normal and cancer cell lines compiled from public gene expression datasets were acquired by the Affymetrix U133A and U133 Plus2 microarray platforms. We used the GENT2 database for the transcription expression validation of CD11b gene in normal and cancer cell lines. For statistical analysis of significance, student t-test was used and p value of <0.05 was regarded statistically significant.

Analysis of EMT score of primary keratinocytes

EMT scores were calculated from the transcriptome data for all the samples and computed using the previously published EMT signature and the two-sample Kolmogorov-Smirnov-based method (Tan et al., 2014; Yadavalli et al., 2017). Gene expression data was mapped to the generic cell line based EMT signature genes (total = 218; epithelial = 170 and mesenchymal = 48) derived using gene expression profiles from tumor and cell lines from various cancers. First, the empirical cumulative distribution function (ECDF) was estimated for Epithelial and Mesenchymal gene sets. Then 2KS test was employed to compute the difference between Mesenchymal ECDF and Epithelial ECDF. The 2KS score was considered as the EMT score. A sample with a positive EMT score and significant p value exhibits a more Mesenchymal phenotype, whereas a negative EMT score and significant p value reflects a more Epithelial phenotype. A sample with insignificant p value is considered intermediate.

Western blot analysis

The keratinocyte lysates were prepared in RIPA buffer with protease inhibitors (Sigma, #P2714) and sonicated at 4°C. Protein lysate was then mixed with 4X Laemmli sample buffer and heated at 95°C for 3 min before loading on the polyacrylamide gel. This was later transferred onto a nitrocellulose membrane. After the transfer, the membrane was blocked using either 5% BSA in Tris buffer Saline containing 0.1% Tween (TBST) for phosphorylated proteins or 5% Blotto (Santa Cruz Biotechnology, sc-2325) for 60 min. The blots were probed overnight with the respective primary antibody (Table S2). After washing with TBST, the blots were probed with HRP-tagged secondary antibodies and washed again. Signals were detected using Enhanced Chemiluminescence substrate (ECL, Merck) and iBright FL (Thermo) detector. The bands were quantified using Fiji (ImageJ) software and normalized to loading controls.

Immunostaining and histology

Skin tissues were either fixed in Bouin's solution, dehydrated, and embedded in paraffin or immediately embedded in OCT (Leica). For staining the OCT sections, 10 -15 μm-thick sections were fixed in 4% paraformaldehyde (PFA) before proceeding to the primary antibody staining. Refer the Table S2 for the list of primary antibodies used and their respective dilutions. Alexa Fluor 488– or Alexa Fluor 568–labelled secondary antibodies (Jackson ImmunoResearch) were used at a dilution of 1:300. DAPI or Hoechst stain was used to mark nucleus. For paraffin tissue staining, the sections were rehydrated followed by antigen retrieval in 10mM sodium citrate buffer (pH 6). 3% H_2O_2 incubation was performed after primary antibody incubation and HRP-labelled secondary antibodies (Jackson ImmunoResearch) was used for IHC. Development was done using DAB substrate (Vector Laboratories; SK4105) to manufacturer's instructions. For secreted protein staining, the use of detergent was completely avoided to prevent permeabilization, and K5 staining was used as an internal control. Imaging was done on an Olympus IX73 microscope or FV1000 confocal microscope and analyzed on the Fiji software.

Flow cytometry

Cells were analyzed by flow cytometry after detachment with Versene at 37°C for 15 min. The cells were centrifuged at 300g for 5 min and then the supernatant was discarded. This was followed by resuspending the cell pellet in room temperature FACS buffer (1% BSA in PBS) and the cells were counted. Approximately $1x10^6$/ml cells were used for analysis. Cells were incubated with 100 μL of diluted fluorescently labeled antibody in FACS buffer on ice for 20 min, followed by centrifugation at 300g for 5 min. The supernatant containing unbound antibody was removed and cells were washed 1 time in 500 μL of cold FACS buffer. The cell pellet was resuspended in ice-cold FACS buffer and stored at 4°C in the dark until analysis.

Fluorescence-activated cell sorting

P9 pups from wild type and Snail Tg animals were sacrificed and the hair was removed using hair removal cream. The skin obtained from the animals were treated with 1mg/ml of dispase overnight at 4°C to separate the epidermis from dermis. The epidermis separated from the dermis was treated with 1X Trypsin to dissociate the epidermal cells for 15min at 370C. The cells were passed through a 70um strainer and washed with FACS buffer (1% BSA in PBS). The cells were stained with Alpha 6 integrin and the staining was performed as mentioned in the Flow cytometry section. The cells were sorted using BD FACS ARIA Fusion.

Calculation of nuclear to cytoplasmic ratio (NCR)

Primary keratinocytes and A388 cells were cultured on collagen (Millipore) coated coverslips and fixed with 4% PFA. Cells were stained with Wheat Germ Agglutinin-Alexa fluor 488(WGA) (Invitrogen) without permeabilising them. After washes with 1xPBS, cells were stained with DAPI and mounted with 80% glycerol. Images of the cells were obtained on Olympus IX73 microscope. Using the Fiji software, areas of the entire cell (by marking the outline of the cell using WGA as reference) and nucleus (with DAPI as reference) were obtained. Cytoplasmic area was calculated by taking the difference between the cell area and nuclear area. With these measurements, the ratio of nuclear area to cytoplasmic area was calculated.

Colony formation assay

Self-renewal of cells was measured by colony formation assay as described in (Franken et al., 2006). Briefly, single cells of keratinocytes or cSCC were seeded at a very low-density of 1000 cells/well for each seeding in a 6-well dish and were allowed to form colonies for 7 days. Colonies were counted under a microscope and were trypsinized for the next seeding. Colony forming assay with recombinant Mindin was done as mentioned above by treating cells with 80ng/ml to 400ng/ml of Mindin. Similarly, cells were seeded upon counting and let to adhere for 8-12hr before treating with 20μg/ml of CD11b inhibitory antibody or its isotype control (Rat IgG). 4 h post inhibitory antibody addition, recombinant Mindin was added, and the cells were allowed to form colonies for 7 days.

Xenograft assay

Primary keratinocytes (WT and *Snail* Tg) and cSCC cell lines (EGFP ctrl and *Mindin* KD) were cultured and $0.25x10^6$ cells were used per injection for each graft. 1:1 ratio of cells in media to Matrigel with reduced growth factors (Corning) was prepared on ice. 2 months old male NSG animals (The Jackson Laboratories) which were maintained and bred at the animal facility at the NCBS under specific pathogen–free conditions, were used for this assay. Cells prepared in Matrigel were injected subcutaneously in the right flank region of the mice. Animals were monitored for tumor development. 8 weeks post injection, animals were sacrificed, and the tumors were collected, and measurements were taken. Tumor volume in mm^3 was calculated using the formula; Volume = [(lengthXwidth^2)/2]. The tumors were subsequently dissociated into single cells using Dispase (Invitrogen) and trypsin (Sigma) and serially grafted.

shRNA mediated knockdown

All lentivirus production and transduction experiments were done in the BLiSC BSL-2 facility. HEK293T cells were well cultured in a 10cm dish till they were 70–80 percent confluent. The cells were then co-transfected with three plasmids-shRNA-pZip-mEf1a (5 μg), psPAX2 (3.75 μg), and pMD2.g (1.25 μg) (total DNA - 10μg) using Lipofectamine LTX reagent (Invitrogen). For transfection, the above-mentioned amounts of DNA were suspended in 500μL plain DMEM to which10μl of plus reagent was added. Meanwhile, 30μL Lipofectamine LTX reagent was dissolved in 500μL plain DMEM in another tube. After incubating 10 min at RT, DNA suspension was added to LTX reagent suspension. The mixture was incubated for 15–20 min. Fresh DMEM with 10% FBS (5 mL) was added to the HEK293T cells, and the transfection mixture was added dropwise the cells with fresh medium. The media was changed 12–16 h post transfection. The Lentivirus was cultivated 24hrs, 48hrs and 72hrs post first media change and all collections were pooled. The presence of lentivirus was tested using lenti go-stix. The virus was concentrated in a 100KDa Amicon centrifugation unit (Merck) at 5000g for 15 min to achieve a 10-fold concentration. The concentrated lentiviral particles were then titrated and added on mouse keratinocytes for infection. 72h post infection %GFP + cells were estimated. Titer that gave 50–60% transduction efficiency was then used for further downstream experiments. For all downstream experiments 72h post infection cells were exposed to puromycin selection (1μg/ml) for 4 days. shRNA constructs against mouse c-Src, Fyn and Yes was procured from Transomics in vector pZIP-mEf1a. For the sequences refer Table S2.

CRISPR/Cas9 mediated *Mindin* knockdown in cSCC cells

CRISPR/Cas9 tool was used to knockdown *Mindin* in cSCC cells (cSCC-KD). The Lentiviral backbone transfer plasmid p-lenti-CRISPR - EGFP sgRNA 1 (Addgene Cat #51760) was used to express human codon-optimized Cas9 protein. The puromycin resistance in this plasmid utilizes EFS promoter and an EGFP targeting synthetic single-guide RNA (sgRNA) element from U6 promoter. This plasmid was used as the negative control in our study. The viral packaging plasmid psPAX2 (Addgene Cat# 12,260) and viral envelope plasmid pMD2.G (Addgene Cat# 12,259) were purchased from Addgene USA.

Plasmid engineering

The EGFP sgRNA 1 sequence of p-lentiCRISPR - EGFP sgRNA 1 plasmid has been replaced by customized *Mindin* specific single-guide RNA (sgRNA) M226R CCGCGCATAGCTCCGACTACAGC (226 nucleotide regions of NM_012445.4:44–1039 Homo sapiens spondin 2) using Quick change mutagenesis with h-M226RgRNA RP (CGCATAGCTCCGACTACAGCGGTGTTTCGTCCTTTCCAC) and h-M226RgRNA FP (GCTGTAGTCGGAGCTATGCGGTTTTAGAGCTAGAAATAGCAAGTTAAAATAAG). The plasmid was further confirmed with sequencing. This transfer vector plasmid is named as p-lentiCRISPR-M226R sgRNA.

Lentivirus production and transduction

The Lentivirus production work was performed in the BSL2 facility following the assigned guidelines. ~4 million HEK293T cells were seeded to a 10 cm dish. After a day, the cells were co-transfected with transfer plasmid (6μg), packaging plasmid psPAX2 (3μg) and

envelope plasmid pMD2.G (3μg) using Lipofectamine 2000 Transfection Reagent (Invitrogen). Post 18 h, transfection media was changed with fresh virus production media (DMEM+10% FBS). After 48 and 72 h, the 10 mL media supernatant having lentiviral particles was collected and filtered with 0.45μm membrane. The 20 mL media was further concentrated to 40 times (500 ul). The concentrated viral particles were frozen in 25 mL aliquots in −80-degree deep freezers. Both M226R and negative control lentiviral particles were used further to infect the cSCC cells. The cSCC cells (0.3 million) were seeded into 6 well plates. The cells were treated with various dilutions of lentiviral particles (0, 50, 100, 200, 400 and 500). After 24hr post infection the media was changed with fresh media containing puromycin (1μg/ml). The appearance of resistance foci was observed in various dilutions as compared to zero dilution treatment. The 400th dilution provided single isolated foci which were used for the experiments. The puromycin selected cells were cultured in DMEM media containing 10%FBS and cells were collected for RNA extraction and validation of the knockdown.

Electron microscopy

Skin samples from P7 WT and *Snail* Tg pups were fixed in 2% glutaraldehyde, 4% formaldehyde in 0.05 M sodium cacodylate, and 2 mM calcium chloride and then embedded in EPON resin and processed. Slices were imaged using the MERLIN Compact VP Scanning Electron Microscope in the BLiSC EM facility.

QUANTIFICATION AND STATISTICAL ANALYSIS

The information on statistical tests is provided in the figure legends. Overall, comparisons of two groups were done using a paired Student's *t* test or Mann-Whitney *U* test. One-way ANOVA followed by Tukey's post hoc analysis was used for comparing three or more groups. Two-way ANOVA followed by Tukey's post hoc analysis was used for comparing three or more groups with multiple conditions. GraphPad Prism 6 (GraphPad Software) was used for all statistical analyses. Data represents the mean ± SEM. *p* values of less than 0.05 were considered significant.